creative commons

COMMONS DEED

저작자표시-비영리-변경금지 2.0 대한민국

이용자는 아래의 조건을 따르는 경우에 한하여 자유롭게

- 이 저작물을 복제, 배포, 전송, 전시, 공연 및 방송할 수 있습니다.

다음과 같은 조건을 따라야 합니다:

저작자표시. 귀하는 원저작자를 표시하여야 합니다.

비영리. 귀하는 이 저작물을 영리 목적으로 이용할 수 없습니다.

변경금지. 귀하는 이 저작물을 개작, 변형 또는 가공할 수 없습니다.

- 귀하는, 이 저작물의 재이용이나 배포의 경우, 이 저작물에 적용된 이용허락조건을 명확하게 나타내어야 합니다.
- 저작권자로부터 별도의 허가를 받으면 이러한 조건들은 적용되지 않습니다.

저작권법에 따른 이용자의 권리는 위의 내용에 의하여 영향을 받지 않습니다.

이것은 이용허락규약(Legal Code)을 이해하기 쉽게 요약한 것입니다.

Disclaimer

dCollection

Failure mechanisms of layered $LiNi_xCo_yMn_{1-x-y}O_2$ cathodes for Li-ion batteries

Hyung-woo Lim

Department of Energy Engineering
(Battery Science and Technology)
Graduate School of UNIST

2015

ULSAN NATIONAL INSTITUTE OF SCIENCE AND TECHNOLOGY

Failure mechanisms of layered $LiNi_xCo_yMn_{1-x-y}O_2$ cathodes for Li-ion batteries

A thesis
submitted to the Graduate School of UNIST
in partial fulfillment of the
requirements for the degree of
Master of Science

Hyung-woo Lim

12. 16. 2014

Approved by

Kyu T. Lee

Major Advisor
Kyu Tae Lee

ULSAN NATIONAL INSTITUTE OF SCIENCE AND TECHNOLOGY

Failure mechanisms of layered $LiNi_xCo_yMn_{1-x-y}O_2$ cathodes for Li-ion batteries

Hyung-woo Lim

This certifies that the thesis of Hyung-woo Lim is approved.

12. 16. 2014

Signature

Thesis supervisor: Kyu Tae Lee

Signature

Professor: Yoon Seok Jung

Signature

Professor: Sung You Hong

ULSAN NATIONAL INSTITUTE OF
SCIENCE AND TECHNOLOGY

Abstract

As the promising cathode material, Ni-containing layered Li NCM oxide has several advantages; low-cost, high capacity, etc. but hard to commercialize because of its poor cycle performance.

About this, many researchers studied the failure mechanisms and regard the surface part problems as the failure mechanism of layered LI NCM oxide.

However, apart from surface part problem, there are other failure mechanisms affect to the poor cycle performance of Li NCM. Among them, we focus and suggest new kinds of failure mechanism; Ni disordering as bulk part problem. To identify, at first, the half cell test shows that the poor cycle performance of Li NCM in several factors, and the degree of Ni disordering during cycling is analyzed using Rietveld refinement method. As results, when the Ni disordering is increased during cycling, the capacity of Li NCM is decreased more and more, and this indicates that Ni disordering can affect the cycle performance of Li NCM during cycling, so it is demonstrated that the Ni disordering is one of the failure mechanism of poor cycle performance of layered LI NCM.

Moreover, we suggest new type solution to improve; Mg doping at Li layer of Li NCM. Several analyses, such as TEM, refinement data show the Mg is successfully doped into Li layer, and the half cell test shows its better cycle performance than bare Li NCM (1C, 30℃). Also, through refinement analysis of cycled Mg-doped Li NCM electrode, we observe that the Ni disordering is also inhibited somewhat, comparing the bare Li NCM results.

ULSAN NATIONAL INSTITUTE OF SCIENCE AND TECHNOLOGY

Contents

ULSAN NATIONAL INSTITUTE OF SCIENCE AND TECHNOLOGY

List of figures

ULSAN NATIONAL INSTITUTE OF SCIENCE AND TECHNOLOGY

ULSAN NATIONAL INSTITUTE OF SCIENCE AND TECHNOLOGY

1. Introduction

In Li cathode material, Ni-containing layered $LiNi_xCo_yMn_{1-x-y}O_2$ (Li NCM) is one of the promising alternatives of commercialized $LiCoO_2$ due to low-cost, high capacity. However, this layered Li NCM has severe capacity fading problem during cycling.

About this problem, many researchers investigated and found several failure mechanisms; Transition metal dissolution, SEI formation, etc.., and these were regarded as the reasons affected to capacity fading problem of layered Li NCM. However, in most of failure mechanism investigations, they are focused only in surface problems, that is, no one paid attention to bulk problems as one of the failure mechanisms of capacity fading problem.

Therefore, in this paper, we demonstrate that the bulk problem, especially Ni disordering, can be one of the failure mechanisms of capacity fading problem using Rietveld refinement analysis. Moreover, to solve Ni disordering problem, we suggest new type of solution; Mg-doping at Li layer, to improve their cycle performance at high C-rate.

1-1. Li-ion battery

In battery research history, the development of Li-ion batteries is one of the most innovative situations. Comparing with previous battery systems, Li-ion battery, especially Li-ion has various advantages; high electropositivity (-3.04V vs. standard hydrogen electrode), light & small metal (equivalent weight M = 6.94 $g \cdot mol^{-1}$, specific gravity ρ = 0.53 $g \cdot cm^{-3}$), etc. And so, Li-ion battery system can get high energy density.[1,2]

These advantages from using lithium metal were first demonstrated and primary Li batteries were developed for commercialization during the 1970s. In this period, due to the strong research effort, it was started to convert Li primary cells into rechargeable cells with high energy density. For example, in 1972, TiS_2 as the cathode material was used by Exxon, with Li metal as anode and Li perchlorate in dioxolane as electrolyte. However, these rechargeable cells with Li metal anode had serious safety problems caused by forming dendrites and powder deposits on recharging. To overcome these safety problems, several modifications were researched, and finally, the new type of battery; $LiCoO_2$ as cathode and graphite as anode first commercialized by Sony Co. in 1991, and since then, C-$LiMO_2$ has became the leading Li-ion battery system using various batteries. The basic diagram of C-$LiMO_2$ battery is illustrated in Figure 1.[3,4]

Figure 1 shows the main cell reaction which is reversible charge-discharge cycles between two layered compounds. In cathode, the cathode reactions are;

$$Li_{1-x}MO_2 + xLi^+ + xe^- \leftrightarrow LiMO_2$$

Because the source of lithium in Li-ion batteries is cathode material, it ensures very prolonged shelf life & excellent safety, compared to Li metal-based batteries. The first process is charging, that is, oxidation and delithiation of $LiMO_2$ in parallel to the reduction and lithiation of graphite. In graphite anode, the anode reactions are;

$$Li^+ + C_6 + e^- \leftrightarrow LiC_6$$

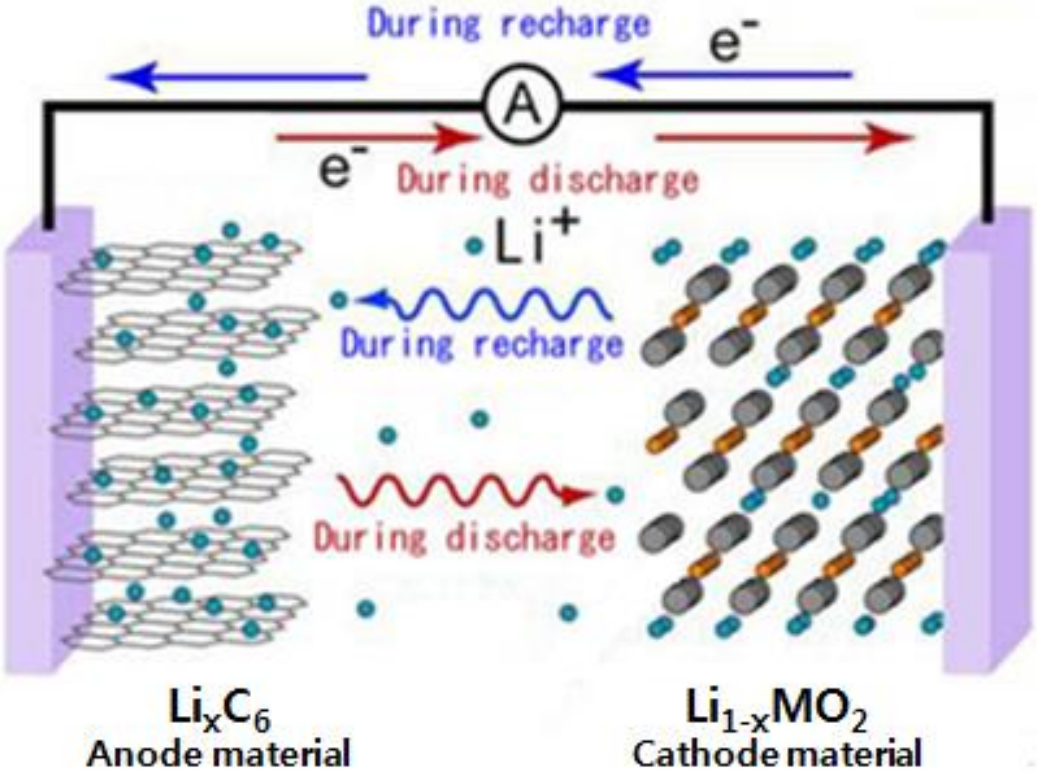

$$\text{Cathode: } Li_{1-x}MO_2 + xLi^+ + xe^- \leftrightarrow LiMO_2$$
$$\text{Anode: } Li^+ + C_6 + e^- \leftrightarrow LiC_6$$

Figure 1. A schematic illustration of Li-ion battery; graphite anode and $LiMO_2$ cathode

1-2. Li layered cathode material

As shown in Figure 2, several oxides with $LiMO_2$ (M = Mn, Co, Ni) crystallize in layered structure of O-Li-O-M-O along c axis which Li^+ and M^{3+} ions occupy the alternate (111) planes of rock salt structure. This structure is O3 layer structure which is the unit cell consisted of Li^+ ions occupy the octahedral sites and three MO_2 sheets. In this structure, reversible extraction-insertion of Li ions in Li planes is allowed by strong-bonded MO_2 layers. The interconnected Li-ion sites; the edge-shared MO_6 octahedral sequence with direct M-M interaction provide good electronic conductivity σ_c depending on the M^{+3} ions' electronic configuration, and the edge-shared LiO_6 octahedral sequence between MO_2 layers provide high σ_{Li} with fast two-dimensional Li ion diffusion. As a result, the crystallized O3 structure $LiMO_2$ oxides is promising candidates for cathode materials.

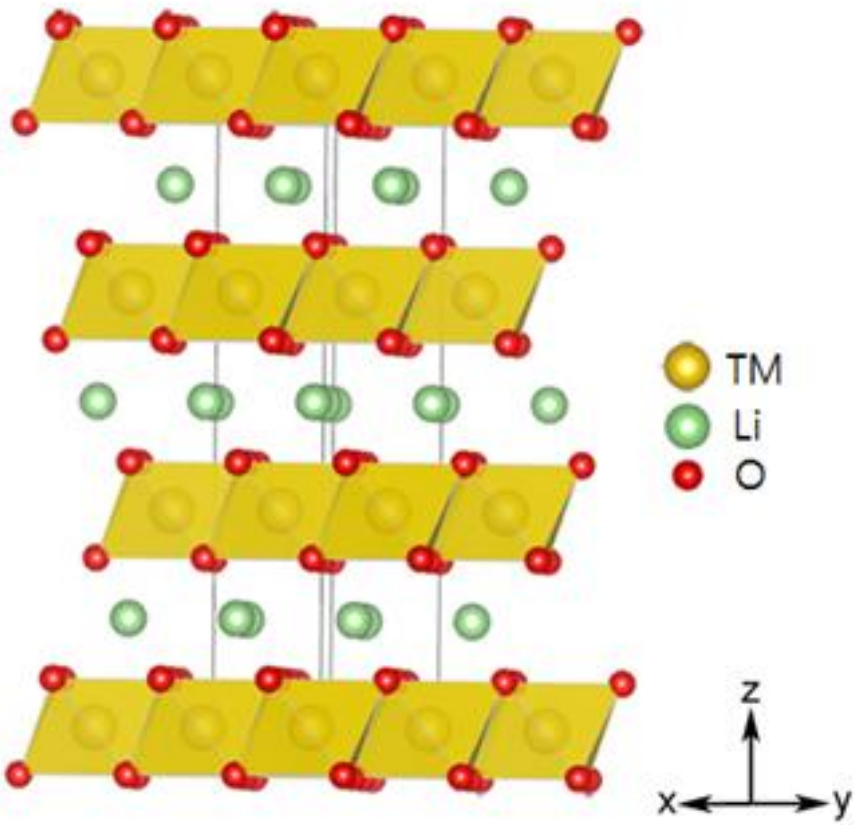

Figure 2. Crystal structure of $LiMO_2$

(1) $LiCoO_2$

Among the layered metal oxide, $LiMO_2$, $LiCoO_2$ is one of the most predominant cathode materials in commercially available Li-ion batteries, because of its high energy density, high accessible Li diffusion pathway, and good cycle performance. However, although it has high theoretical capacity (273 $mAh \cdot g^{-1}$), the practical capacity is limited to about 140 $mAh \cdot g^{-1}$ because of its phase transformation from hexagonal to monoclinic phase between 4.1 and 4.2V ($LiCoO_2 \Rightarrow Li_xCoO_2$ ($x < 0.5$)) (Figure 3).[5-10] Also, this phase transformation leads to volume change along the c axis (~2% expansion), which extends defects (micro-cracks) of particles, disconnects electrical contact of particles, and increases cell capacity fading.[11]

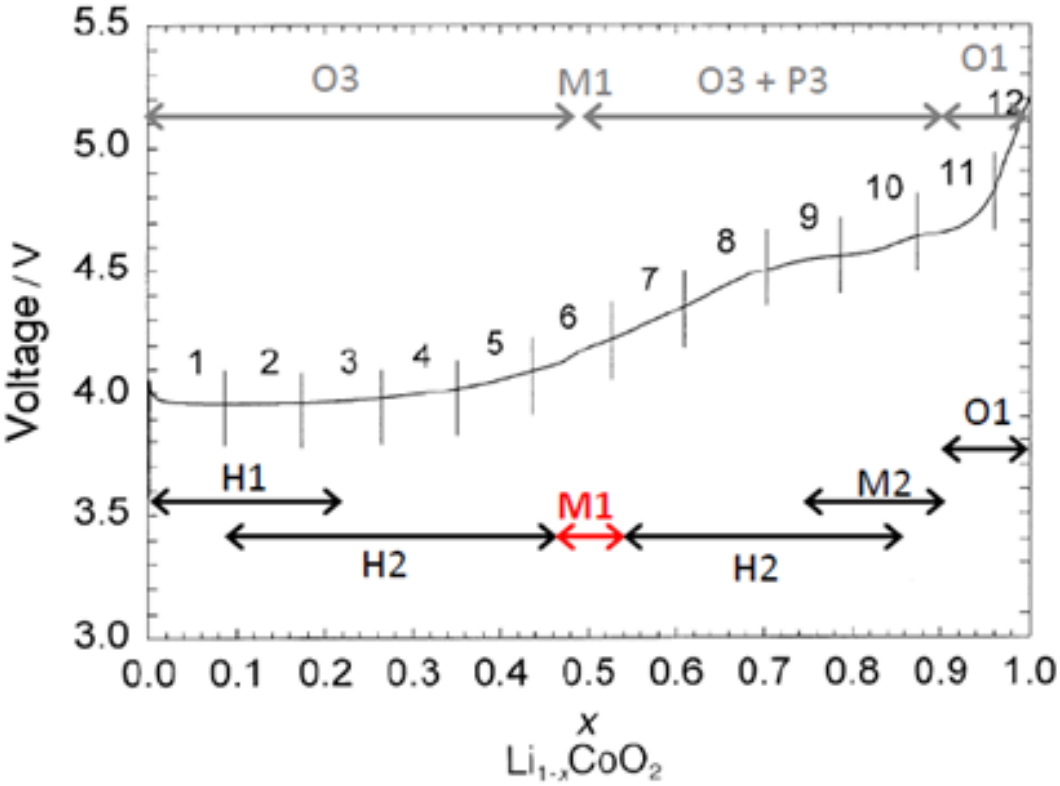

Figure 3. First charging curve of a Li | $Li_{1-x}CoO_2$ cell at the C/10 rate from 3.5 to 5.2 V

ULSAN NATIONAL INSTITUTE OF SCIENCE AND TECHNOLOGY

(2) $LiNi_xCo_yMn_{1-x-y}O_2$

Studies to overcome the disadvantages of $LiCoO_2$; high-cost, low capacity, etc approaches to $Li[Ni,Co,Mn]O_2$ that considered as compensation Co metal's disadvantage with others' advantage.[12] For example, $LiNi_{1/3}Co_{1/3}Mn_{1/3}O_2$, the first commercialized Li NCM cathode material, better rate capability and structural stability.[13-26]

Among them, $LiNi_xCo_yMn_{1-x-y}O_2$ ($x \geq 0.4$) received much attention due to its better electrochemical performance and higher capacities, caused by high Ni composition. In $LiNi_xCo_yMn_{1-x-y}O_2$ ($x \geq 0.4$), these have different electrochemical & structural properties with various composition of Co & Mn. Because high Ni composition usually results in poor cycle performance & structural instability, the best compositions of metal ions is not yet clearly understood, so many studies have been carried out.[27] However, in commercialization of Li-ion battery, thermal instability & structural collapse during long-term cycling is still an obstacle.[28,29] In detail, this problem is caused by exothermic reactions with electrolyte, oxygen release at elevated temperature (55℃), simultaneously.[30] To stabilize without capacity loss, various cation substitutions have been studied.[31-34]

1-3. Failure mechanisms of $LiNi_xCo_yMn_{1-x-y}O_2$

As we mentioned, in $LiNi_xCo_yMn_{1-x-y}O_2$ ($x \geq 0.4$), there are poor cycle performance & structural instability during cycling. About this problem, some researchers have investigated and suggested several failure mechanisms; Transition metal (Ni, Co, Mn) dissolution,[35] Residual Li,[36] and Phase transition of cathode surface.[37]

(1) Transition metal dissolution

In charge/discharge process, when Li ions move from/to cathode material, the oxidation numbers of transition metal are changed from stable state to unstable state. Because of these changes, layered NCM oxide material becomes unstable, and this leads to the transition metal dissolution from layered NCM oxide cathode material.

After dissolution, these dissolved metals make various side reactions at cathode & anode. Especially, at graphite anode, in full cell, there are self-discharge due to Mn deposition,[38] or solid electrolyte interphase with Ni, Co, and Mn ions are formed. Each metal SEI hinder the Lithium intercalation and lead capacity fading with their unique mechanisms (Figure 4a-c).[35]

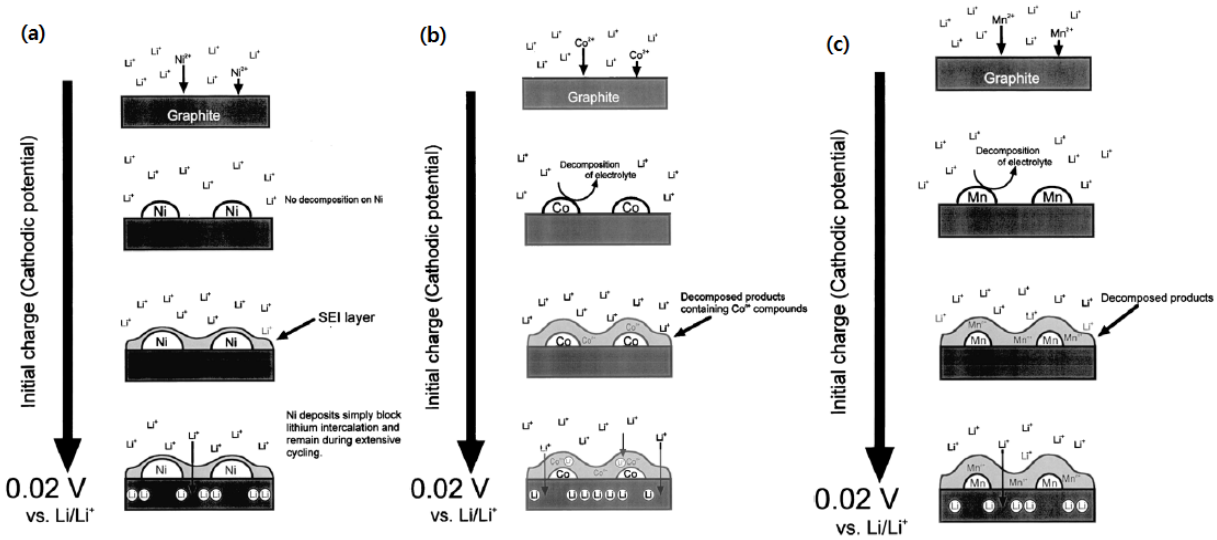

Figure 4. Schematic drawing of the influence of metal addition in electrolyte on the initial charge process of the graphite negative electrode; (a) Ni(Ⅱ) (b) Co(Ⅱ) (c) Mn(Ⅱ)

ULSAN NATIONAL INSTITUTE OF SCIENCE AND TECHNOLOGY

(2) Residual Li contents

On the surface of $LiNi_xCo_yMn_{1-x-y}O_2$, especially high Ni composition, as the cathode material, there are Li_2CO_3 and LiOH resulting from reaction with air.[39,40] These residual Li contents lead to degrade layered NCM's capacity; LiOH generates acidic HF in electrolyte caused by reaction with $LiPF_6$, and Li_2CO_3 make severe swelling at high temperature, especially in charge process.[41]

Figure 5a·b shows the relationship between capacity fading problem and amount of residual Li contents. The amount of total residual Li contents increased drastically with increasing Ni contents of layered NCM oxide (Figure 5a), and these Ni-rich layered NCM oxide has poorer cycle performance (Figure 5b).[36]

(a)

	LiOH	Li_2CO_3	Total
$Li[Ni_{1/3}Co_{1/3}Mn_{1/3}]O_2$	790	1008	1798
$Li[Ni_{0.5}Co_{0.2}Mn_{0.3}]O_2$	1316	1080	2396
$Li[Ni_{0.6}Co_{0.2}Mn_{0.2}]O_2$	2593	2315	4908
$Li[Ni_{0.7}Co_{0.15}Mn_{0.15}]O_2$	4514	6540	11,054
$Li[Ni_{0.8}Co_{0.1}Mn_{0.1}]O_2$	10,996	12,823	23,819
$Li[Ni_{0.85}Co_{0.075}Mn_{0.075}]O_2$	11,285	15,257	26,542

(b)

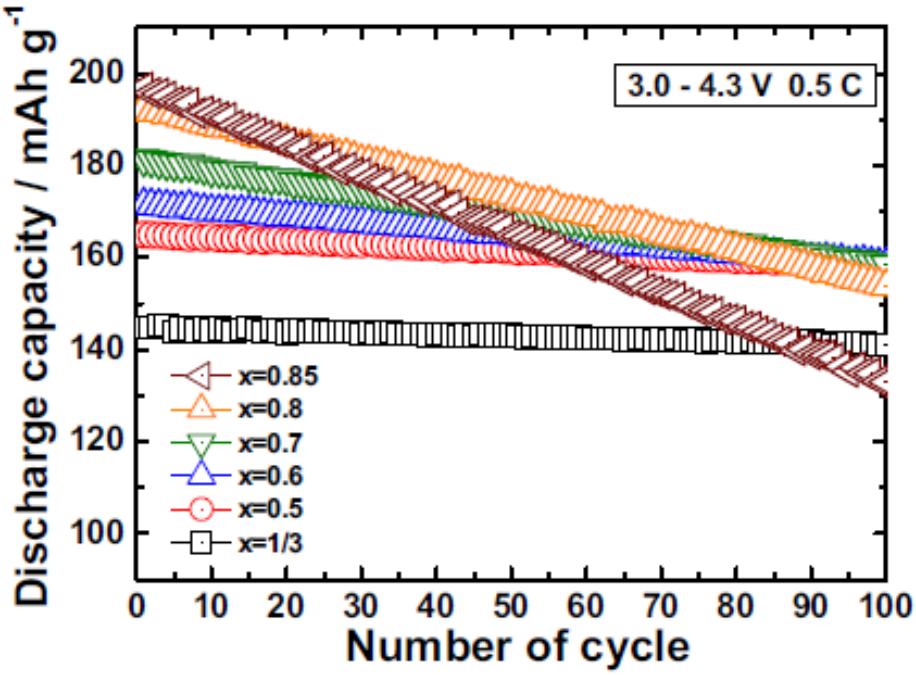

Figure 5. (a) Total residual Li amounts (LiOH and Li_2CO_3) on the $Li[Ni_xCo_yMn_z]O_2$ cathode surface (unit: ppm) (b) Discharge capacity vs. cycle number for the $Li/Li[Ni_xCo_yMn_z]O_2$ (x = 1/3, 0.5, 0.6, 0.7, 0.8 and 0.85) cells at 25℃

(3) Phase transformation of cathode surface

In layered NCM oxide, especially in Ni-rich NCM oxide surface, there is serious phase transformation with increasing cutoff voltage as one of the other failure mechanisms, and Figure 6 shows the schematic diagram of phase transformation of $LiNi_{0.5}Co_{0.2}Mn_{0.3}O_2$. At first, in 4.5V cutoff cycling, the surface of the electrode has phase transformation mainly to spinel phase, with small part of rock salt formation. In addition, in increased 4.8V cutoff cycling, the rock salt phase is more universally formed than 4.5V cutoff, and in result, the rock salt phase encircles the NCM oxide material (Figure 6).[37]

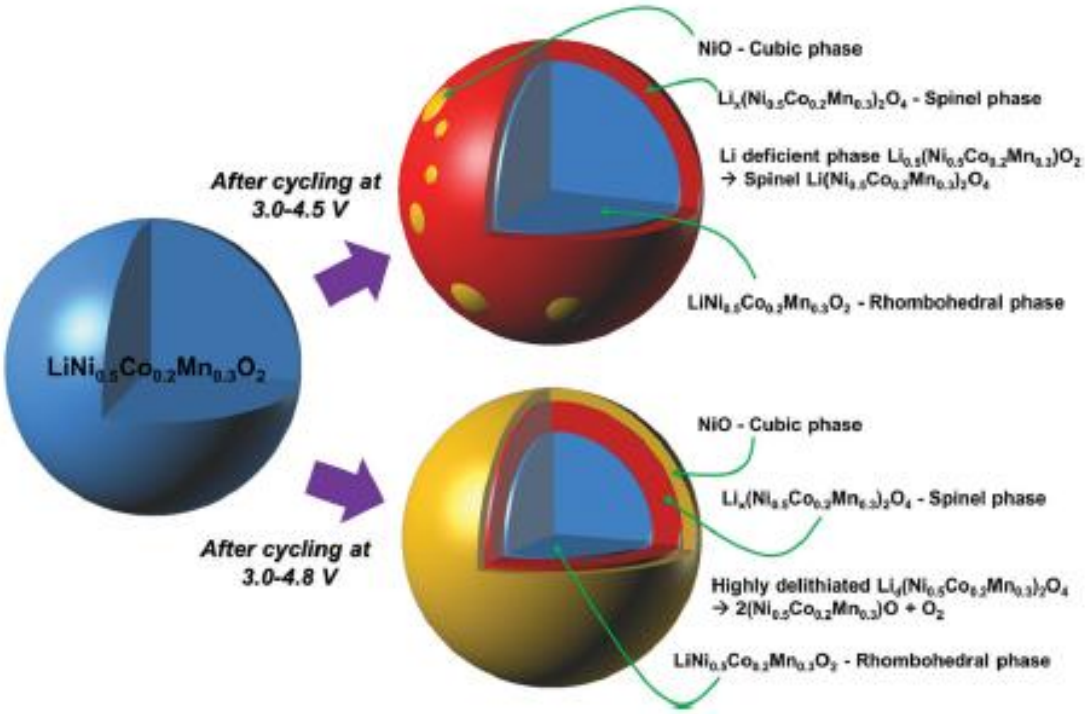

Figure 6. Degradation mechanisms of $LiNi_{0.5}Co_{0.2}Mn_{0.3}O_2$ and phase transformation after cycle tests under high-voltage conditions

ULSAN NATIONAL INSTITUTE OF SCIENCE AND TECHNOLOGY

1-4. My topic

(1) New suggested mechanism; Ni disordering (Bulk part)

Like this, many researchers have investigated and suggested about the failure mechanisms of capacity fading of layered Li NCM oxide, but these investigations have been focused on surface part.

However, the investigation about the other parts of failure mechanisms is insufficient relatively. Therefore, we studied and suggested the new failure mechanism focusing on another part; Ni cation disordering.

Ni cation disordering is the transformation that some Ni ions migrate from the transition metal layer to vacant sites of Li layer. However, in fact, any transition metals in TM layer have possibility to go through the migration.

Figure 7·8 shows the pathways for migration of transition metal ion, M^{n+}, to vacant Li layer. In charged cathode, $Li_{1-x}MO_2$, for transformation to a spinel-like phase, some transition metal ion $M^{3+/4+}$ should migrate from the octahedral sites of M layer (3b sites) to empty octahedral sites of Li layer (3a sites). At this process, migrated transition metals should pass the neighboring tetrahedral sites (T_1 or T_2).[42,43]

ULSAN NATIONAL INSTITUTE OF
SCIENCE AND TECHNOLOGY

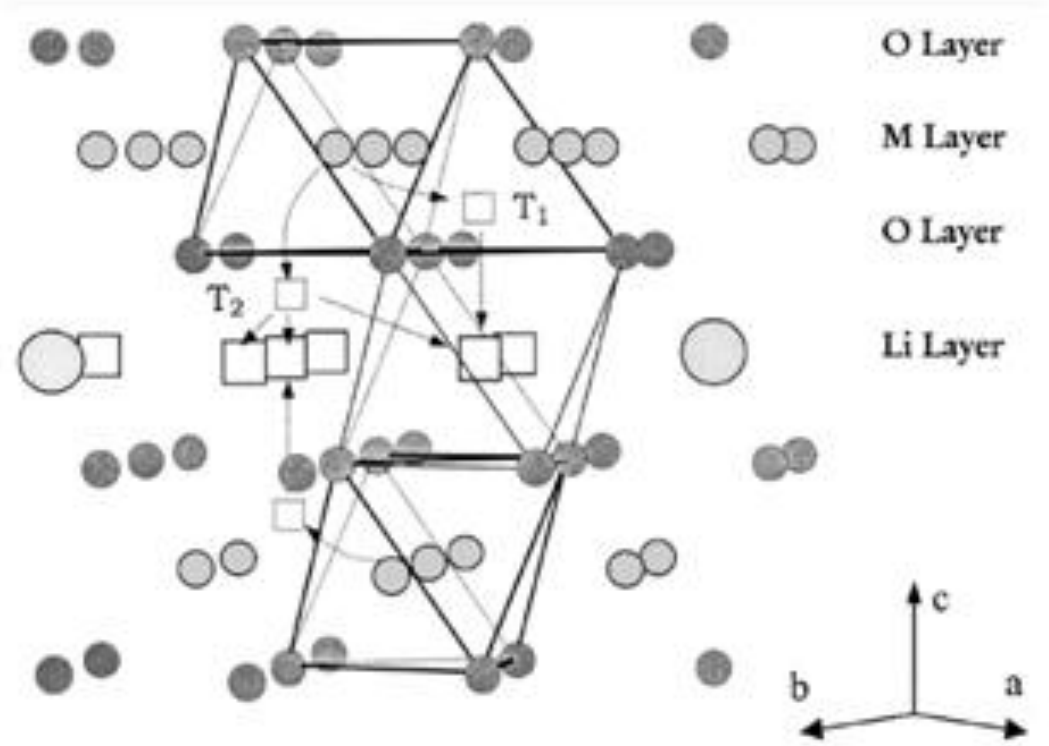

Figure 7. Illustration of the paths for the migration of the transition metal ion M^{n+} from the octahedral sites in the transition metal layer to the octahedral sites in the Li layer via the neighboring tetrahedral sites (T_1 and T_2)

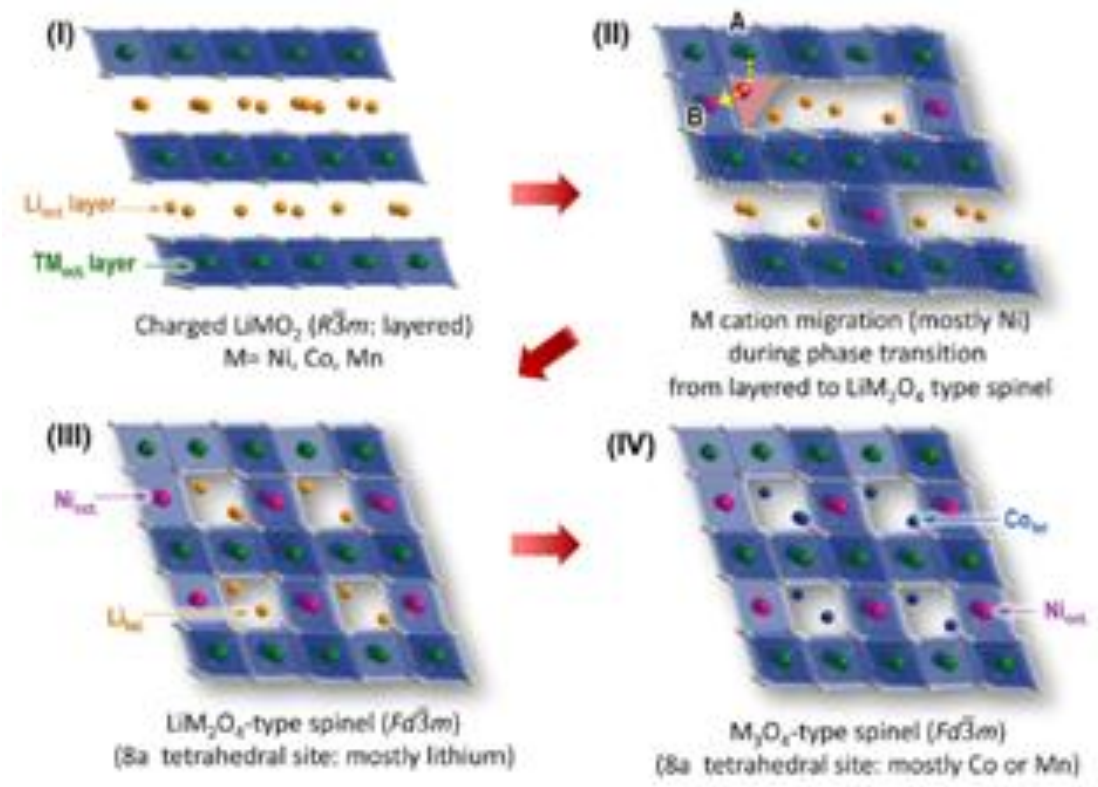

Figure 8. Schematic illustration of phase transition and the possible TM cation migration path in the charged NMC cathode materials during thermal decomposition

Like this, every transition metal have possibility to happen cation disordering, but in real, only Ni ions (Ni^{2+}) occur cation disordering due to its similar radius to Li ions (Li^{+}).

Furthermore, to identify whether Ni cation disordering affects to cycle performance of layered Li NCM cathode, the data of difference of Ni cation disordering during cycling is needed. About this, Figure 9 shows the arrangement change of Li & Ni during charge-discharge process of $LiNi_{0.5}Mn_{0.5}O_2$. According to the paper, in charge process, the composition of Ni is decreased at Li layer, whereas in discharge process, Ni ions come back to Li layer, increasing Ni composition.[44] Resultingly, Ni ions migrate between Li & TM layer during insertion-extraction of Li, and this can be the evidence of Ni cation disordering during cycling.

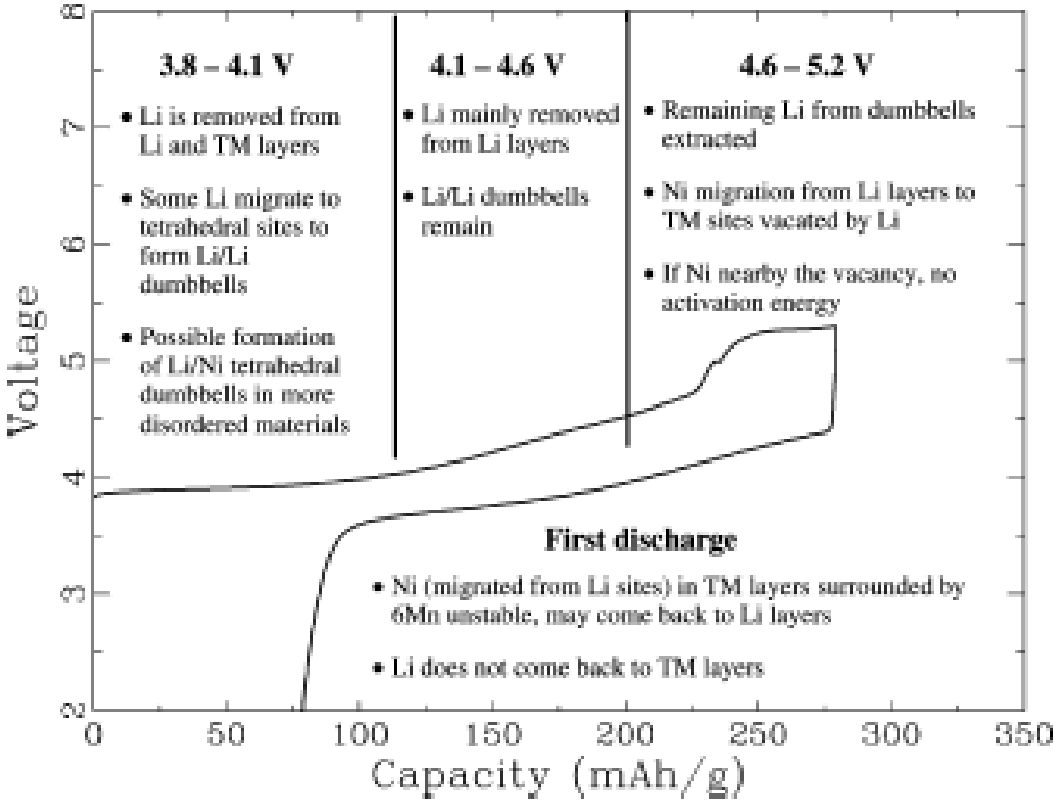

Figure 9. Summary of structural changes during the first cycle between 5.3 and 2.0V of $LiNi_{0.5}Mn_{0.5}O_2$

(2) New solution; Mg-doping at Li layer

In general, to overcome improve layered Li NCM oxide cathode, most researchers used another transition metal doping at transition metal layer or coating processes.

On the other hand, in this paper, we introduce the new-type solution; magnesium ion doping at Li layer of layered Li NCM cathode. In overlithiated layered oxide (OLO), especially Mn-rich OLO, this solution was applied and improved cycle performance due to structural stabilization with expansion of lattice (Figure 10).[45] Similarly, in Li NCM oxide, Mg-doping stabilizes the structure for better cycle performance. Also, because of fixed Mg ions, the Ni disordering process is blocked somewhat.

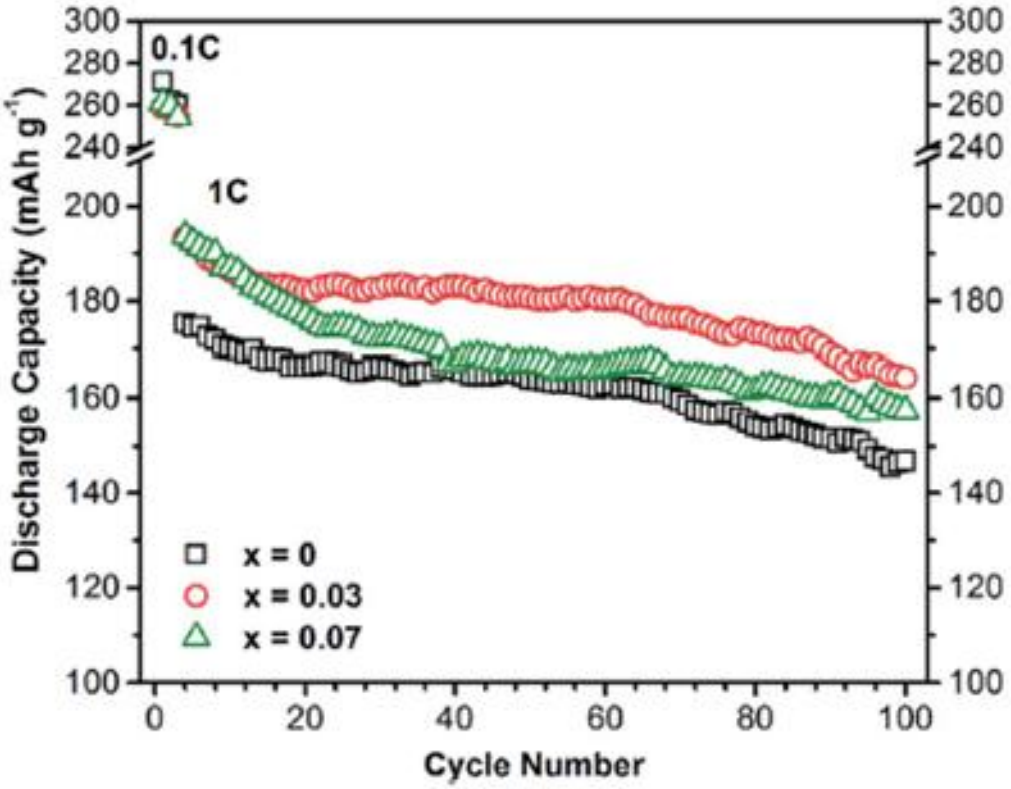

Figure 10. Discharge capacity of the cells with respect to cycle number under 1C for $Li_{1.2-x}Mg_xMn_{0.54}Ni_{0.13}Co_{0.13}O_2$

ULSAN NATIONAL INSTITUTE OF SCIENCE AND TECHNOLOGY

2. Experimental Procedure

2-1. Synthesis of layered Li NCM oxide

To prepare the composite metal carbonate $(Ni_{0.4}Co_{0.2}Mn_{0.4})\cdot CO_3$ and hydroxide $(Ni_{0.6}Co_{0.2}Mn_{0.2})\cdot(OH)_2$ as the precursor, co-precipitation method was employed. The co-precipitation method as follows; First, an aqueous solution with $NiSO_4\cdot 6H_2O$, $CoSO_4\cdot 7H_2O$, $MnSO_4\cdot H_2O$ (molar ratio of Ni : Co : Mn = 4 : 2 : 4 & 6 : 2 : 2, concentration of 2.0 mol·dm^{-3}) was put into continuous stirred tank reactor (CSTR) under N_2 atmosphere.[46-49] Simultaneously, Na_2CO_3 or NaOH solutions as pH controller & NH_4OH solutions as a chelating agent were also put into CSTR. In addition, other conditions; pH, temperature, input amount, and stirring speed were set before start co-precipitation, and during this process, these conditions were monitored and controlled. After co-precipitation, the best-synthesized precursors were filtered, washed, and dried at 80℃, 24h.

And then, obtained precursors were mixed with Li_2CO_3 (molar ratio 1 : 0.5) and heated at 850℃ (carbonate) & 800℃ (hydroxide) for 10h in air atmosphere.

To identify the synthesis of layered Li NCM oxide, several measurements were observed; XRD, SEM, ICP, etc. Powder X-ray diffraction (XRD) data were measured on a Rigaku D/MAX2500V/PC diffractometer using Cu-Kα radiation (λ = 1.5405Å) operated from long scan (2θ = 10~80˚, 0.2˚/min), powder morphology was measured by Cold-SEM, and atomic composition of samples was obtained by ICP spectrometry.

(1) Electrochemical characterization

Synthesized layered Li NCM oxide powders were used as the cathode materials, made by mixing 80wt.% of active materials, 10wt.% of carbon black (Super-P, Timcal Inc.), and 10wt.% of polyvinylidene fluoride (PVdF, KF1000, Kureha Chemical Industry) binder, with coating onto an Al foil. In addition, Li-metal was used as anode material, PE separator was used as the separator, and the electrolyte solution was composed of 1.3M lithium hexafluorophosphate ($LiPF_6$) dissolved in solvents mixed with ethylene carbonate (EC), ethyl methyl carbonate (EMC), dimethyl carbonate (DMC) (volume ratio 3 : 4 : 3).

The coin-type half cells (2032) of layered Li NCM oxide was assembled in argon filled glove box, and galvanostatic experiments were performed at 30 & 60℃ in voltage range; 4.4 and 3.0V (vs. Li/Li^+). In cycle test, it is composed of 1 cycle of pre-cycle (0.1C) and 200 cycles (1C).

ULSAN NATIONAL INSTITUTE OF SCIENCE AND TECHNOLOGY

(2) Failure mechanisms analysis

To identify the relationship between focusing failure mechanism and capacity fading problem, several measurement methods, mainly Rietveld refinement method, were used.

Focusing mechanism; Ni disordering – Rietveld refinement analysis

To analyze the Rietveld refinement data, X-ray diffraction (XRD) data was needed. The coin-type half cells (2032) were assembled at first, then synthesized cycled electrodes following Ni composition (424 vs. 622), cycle number (50 vs. 100 vs. 150 vs. 200), and temperature (30℃ vs. 60℃). After that, XRD data of each samples were measured, and the relationships between Ni disordering and capacity fading problem via Rietveld refinement data.

2-2. Chemical Mg-doping at Li layer

The process about synthesize $Mg_xLi_{1-2x}(NCM)O_2$ is presented in Figure 11. Synthesized layered Li NCM 424 oxide and the mixture with acetonitrile was starting solution. In this solution, excess nitronium tetrafluoroborate (NO_2BF_4) (Sigma-Aldrich) were added, stirred for 2h and filtered for elimination of Li in layered Li NCM oxide. Then, excess sodium iodide (NaI) (Sigma-Aldrich) with acetonitrile were added, stirred for 2h, and filtered for insertion of Na in Li layer. Next, through reflux reaction with acetonitrile solvent and Magnesium bromide ($MgBr_2$) (Sigma-Aldrich) reacted at least 6h and filtered, Na ions in Li layer were changed to Mg ions. At last, Mg-doped Li NCM 424 were calcined at 300℃ for 5h in air.

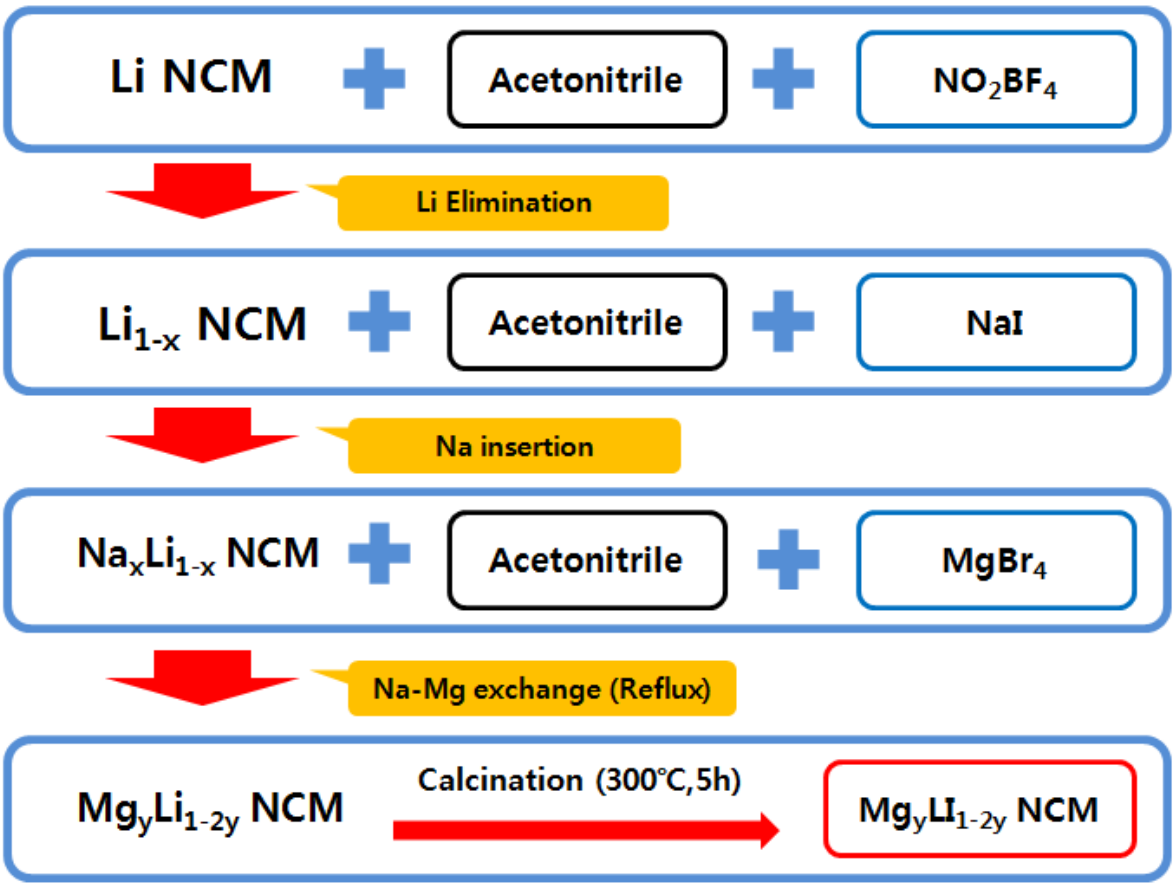

Figure 11. Schematic diagram of chemical Mg doping process in Li layer of layered Li NCM

ULSAN NATIONAL INSTITUTE OF SCIENCE AND TECHNOLOGY

(1) Electrochemical characterization

Similar to 2-1-(1), just different active materials; $Mg_xLi_{1-2x}(NCM)O_2$ (Noheat vs. 300℃ calcination).

(2) Improvement analysis

To identify the synthesis of Mg-doping at Li layer, Transmission electron microscopy (TEM) and Rietveld refinement data of bare $Mg_xLi_{1-2x}(NCM)O_2$ powder were used. Also, to observe the relationship between Ni disordering and Mg-doping effect, Rietveld refinement data of 200 cycled electrode were compared with 200 cycled layered Li NCM electrtode.

ULSAN NATIONAL INSTITUTE OF SCIENCE AND TECHNOLOGY

3. Results & Discussions

3-1. Synthesis of layered Li NCM oxide

Synthesis characterization

To analyze the failure mechanisms of Ni-contained layered Li NCM oxides, identify the synthesis of layered Li NCM oxides (Li NCM 424·622) is the previous step, and to identify, several measurements were used; XRD, SEM, and ICP.

Figure 12a shows the XRD patterns of Li NCM 424·622 bare powder. Comparing to the hexagonal α-$NaFeO_2$ structure with R-3m space group at bottom part, both synthesized Li NCM 424·622 have same peaks. Also, these have the clear splits of (006)/(102) & (108)/(110) doublets. These results indicate that synthesized Li NCM materials formed well-ordered layer structure.[50]

The SEM images for morphology identification of layered Li NCM 424·622 are in Figure 12b·c.

These particles are maintained their spherical morphology comparing with co-precipitated precursor, and particle sizes are similar; 7~10 μm.

The ICP results which are Ni, Co, Mn, and Li composition are listed in Figure 12d. In results, as we expected, each Li NCM materials measure similar to target compositions; the ratio of Ni, Co, Mn & ratio of Li, NCM.

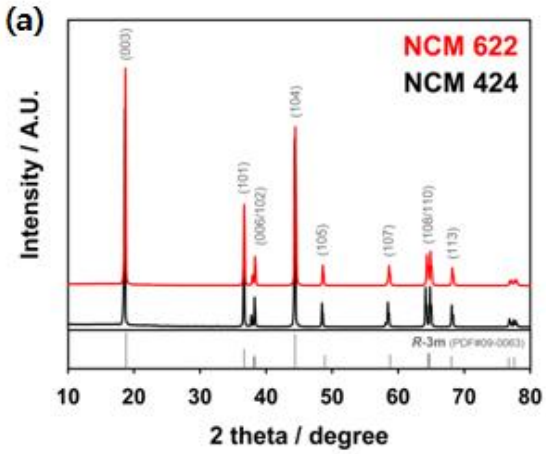

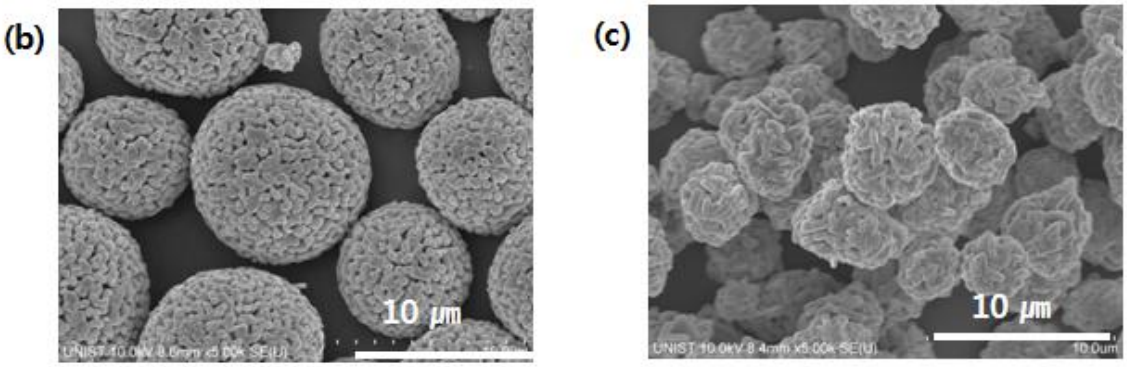

(d)

	Ni	Co	Mn	Li : NCM
Li NCM 424 (Carbonate, 850℃)	0.394	0.212	0.393	0.975 : 1
Li NCM 622 (Hydroxide, 800℃)	0.605	0.198	0.198	0.942 : 1

Figure 12. (a) XRD patterns of synthesized $LiNi_{0.4}Co_{0.2}Mn_{0.4}O_2$ and $LiNi_{0.6}Co_{0.2}Mn_{0.2}O_2$ (b) SEM images of $LiNi_{0.4}Co_{0.2}Mn_{0.4}O_2$ and (c) $LiNi_{0.6}Co_{0.2}Mn_{0.2}O_2$ (d) ICP data of bare powder

ULSAN NATIONAL INSTITUTE OF SCIENCE AND TECHNOLOGY

Electrochemical performance

To observe the electrochemical performance of layered Li NCM cathode, a plot of cycleability for layered Li NCM 424 and 622 cathodes in Li half cells at 30℃ and 60℃ is shown in Figure 13. At 1C rate test, the initial discharge capacities of Li NCM 424 & 622 at 30℃ are 128.7 and 151.8 $mAh \cdot g^{-1}$, respectively. Also, at same rate, the initial discharge capacities of Li NCM 424 & 622 at 60℃ are 165.1 and 175.5 $mA \cdot g^{-1}$, respectively. Thus, at higher Ni composition and reaction temperature condition, the value of initial capacity is increased. However, after 200cycle, the discharge capacities are all decreased; Li NCM 424 at 30℃ (D.C = 78.5 $mA \cdot g^{-1}$, C.R = 60.99%), Li NCM 622 at 30℃ (D.C = 75.2 $mA \cdot g^{-1}$, C.R = 49.54%), Li NCM 424 at 60℃ (D.C = 78.9 $mA \cdot g^{-1}$, C.R = 47.79%), and Li NCM 622 at 60℃ (D.C = 56.9 $mA \cdot g^{-1}$, C.R = 32.42%), but the degree is different. According to these results, in layered Li NCM half cell test, at higher Ni composition and temperature, it has higher initial capacity but poorer cycle performance. In addition, the detailed voltage profiles of half cell test at each condition are shown in Figure 14.

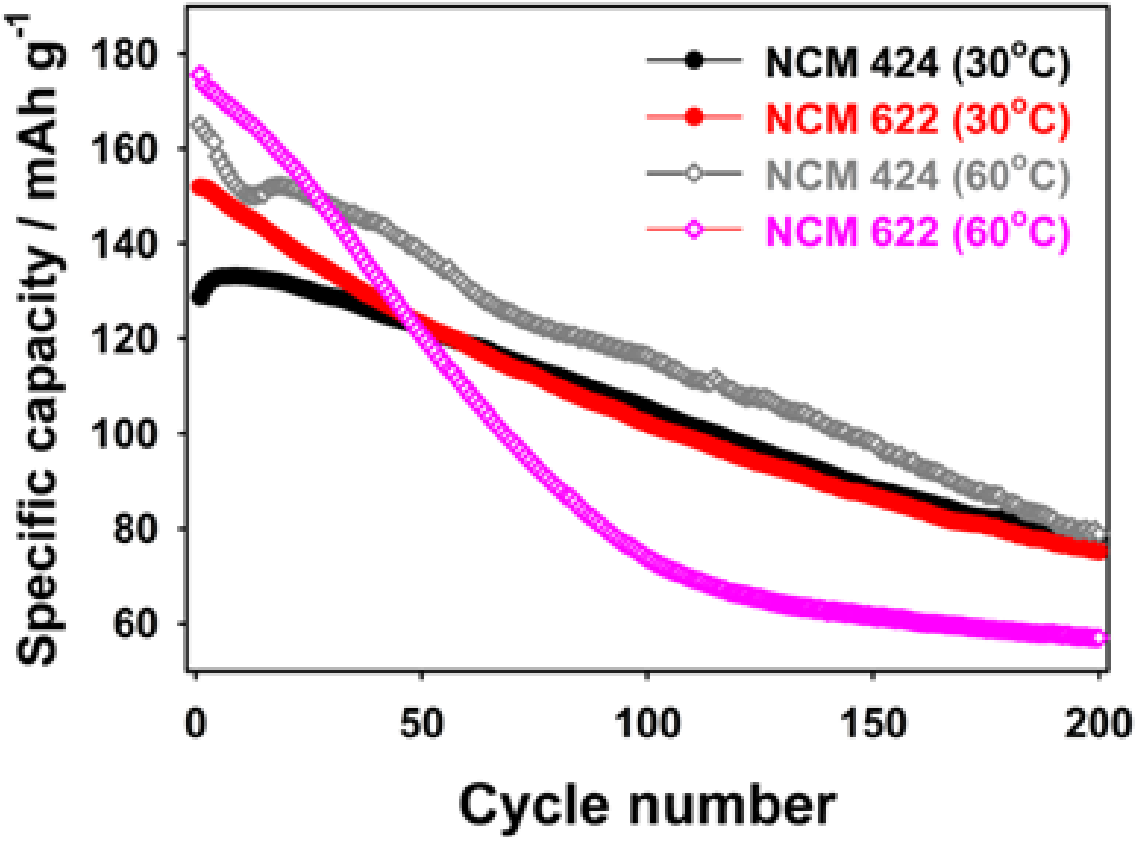

Figure 13. Cycleability of Li NCM 424·622 half cell with Li metal anode at 30℃ & 60℃ (1C rate)

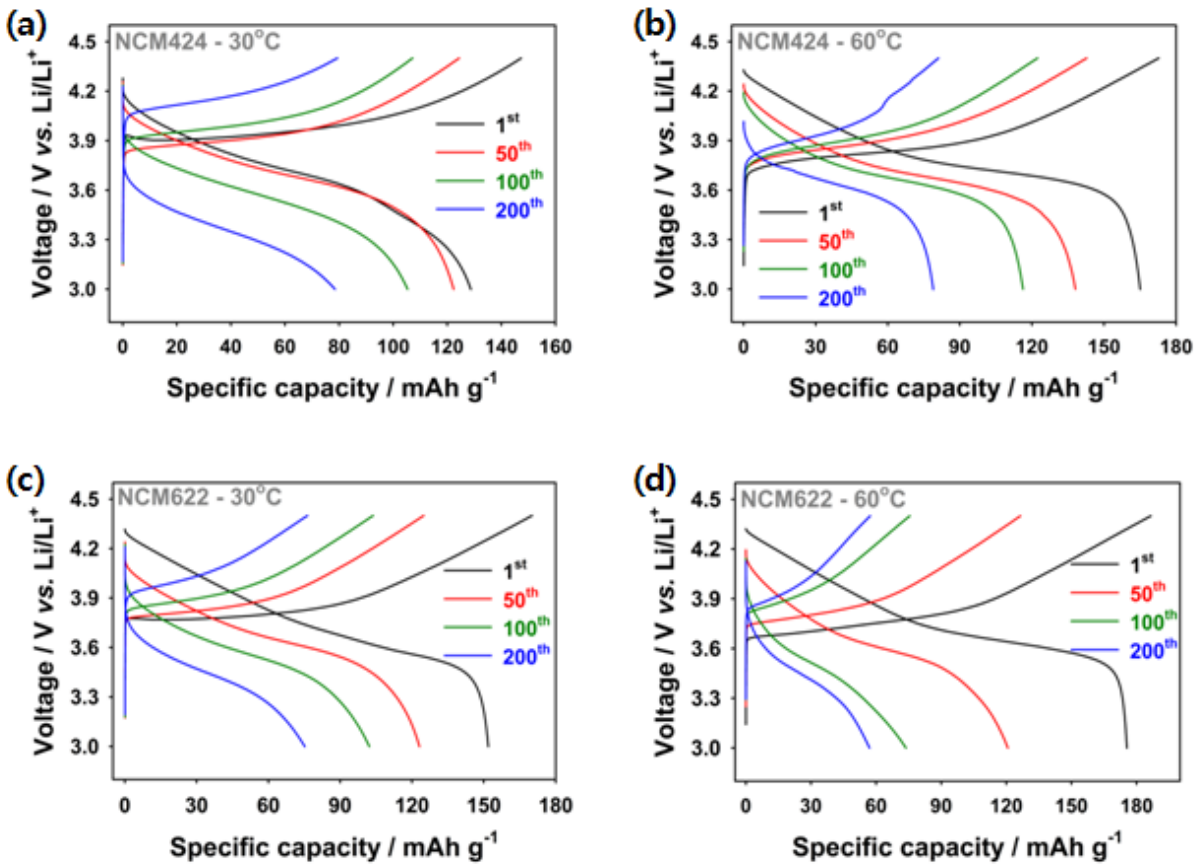

Figure 14. Voltage profile of Li NCM 424·622 half cell with Li metal anode at 30℃ & 60℃ (1C rate)

ULSAN NATIONAL INSTITUTE OF SCIENCE AND TECHNOLOGY

Identification of failure mechanisms

Before the Rietveld refinement analysis, X-ray diffraction (XRD) of cycled electrodes is measured as the raw material for converted refinement data. These XRD data of cycled electrodes are shown in Figure 15. In XRD data, there are several criteria for comparison; temperature (30℃ vs. 60℃) (Figure 15a·b), cycle number (50 vs. 100 vs. 150 vs. 200cycle) (Figure 15c·d) with bare powder XRD data as the reference.

In results of comparison, all cycled Li NCM 424·622 electrode material maintain its intrinsic layered structure, which has some additional peaks, that is the peak of Aluminum foil (●) and Beryllium window (◆), so in result, layered Li NCM 424·622 cathode electrodes preserve their layered structure during cycling.

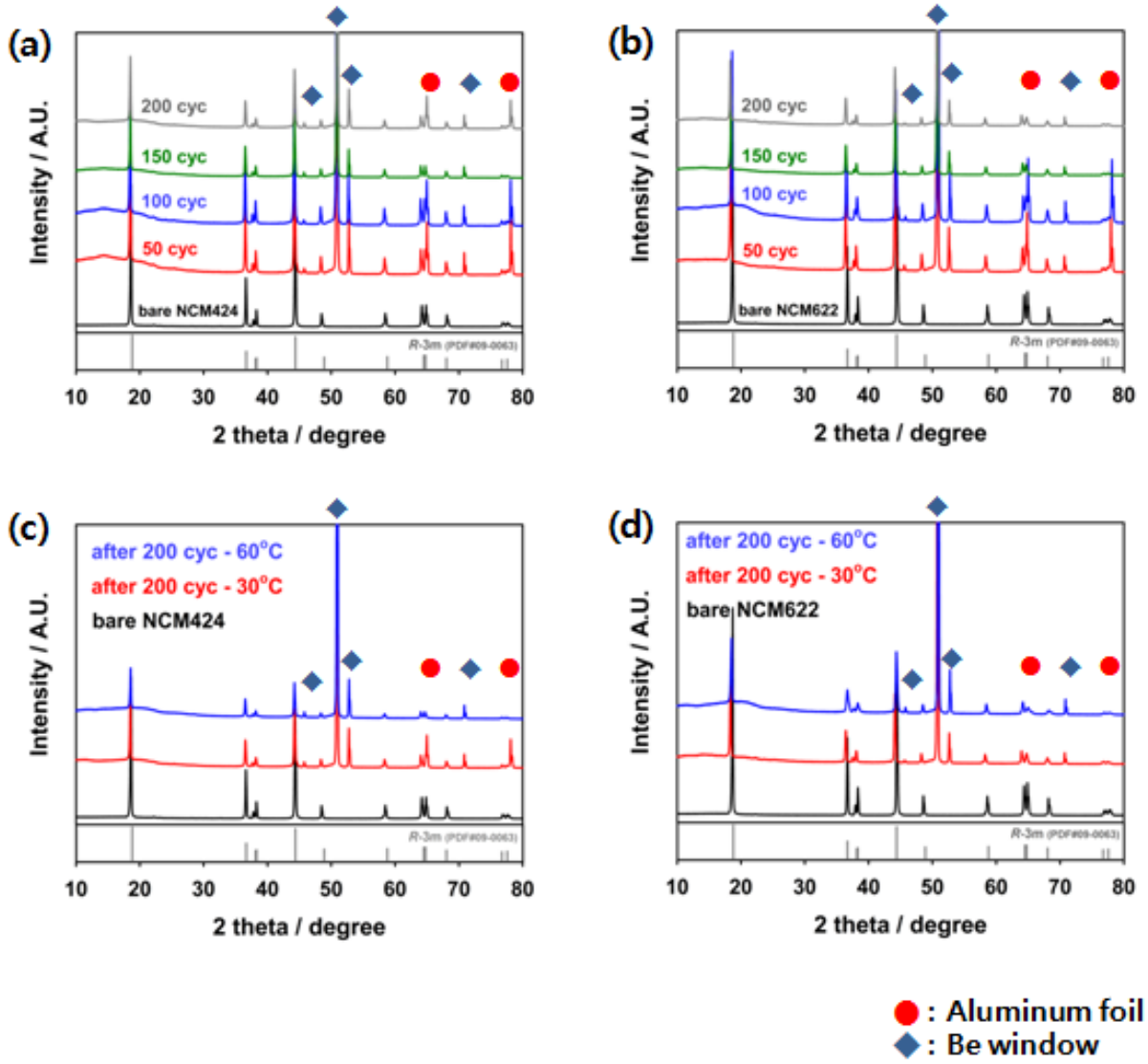

Figure 15. XRD patterns of cycled electrode; (a) LiNCM 424 per cycle number (b) LiNCM 622 per cycle number (c) LiNCM 424 per temperature (d) LiNCM 622 per temperature

ULSAN NATIONAL INSTITUTE OF SCIENCE AND TECHNOLOGY

To identify the degree of Ni cation disordering at each cycled electrodes, the Rietveld refinements method is used comparing with bare powder, and the result values are plotted following cycle number (Figure 16a) and temperature (Figure 16b). At first, comparing bare powder Li NCM 424·622, every cycled electrode has higher value of Ni disordering, and this demonstrates that Ni disordering occurs during cycling.

Also, in Figure 16a, comparing the graph of Li NCM 424 (blue line) versus Li NCM 622 (red line), Li NCM has higher value at spotted cycles, this means that Ni composition is one of the factors of Ni disordering; higher Ni composition, higher Ni disordering value. Another thing, in both 424·622 cases, when the cycle number is increased, the Ni disordering value is also increased. This also means that the cycle number is another factors of Ni disordering; in case the cycle number is increased, there are more severe Ni disordering.

However, as in Figure 16b, there is different result to our expectation, that is higher temperature cycled cathode has lower Ni disordering value in both cases. This means that there is no relationship between the cycle temperature and Ni disordering process.

In result, except temperature, when the cycle number and Ni composition are increased, the degree of Ni disordering is also increased. Furthermore, at these conditions, the discharge capacity of layered Li NCM cathode is decreased severely. Through these results, therefore, Ni disordering and capacity fading of layered Li NCM has relationship during cycling, and that is, Ni disordering can be one of the failure mechanisms in layered Li NCM cathodes as the bulk-structural problem.

ULSAN NATIONAL INSTITUTE OF
SCIENCE AND TECHNOLOGY

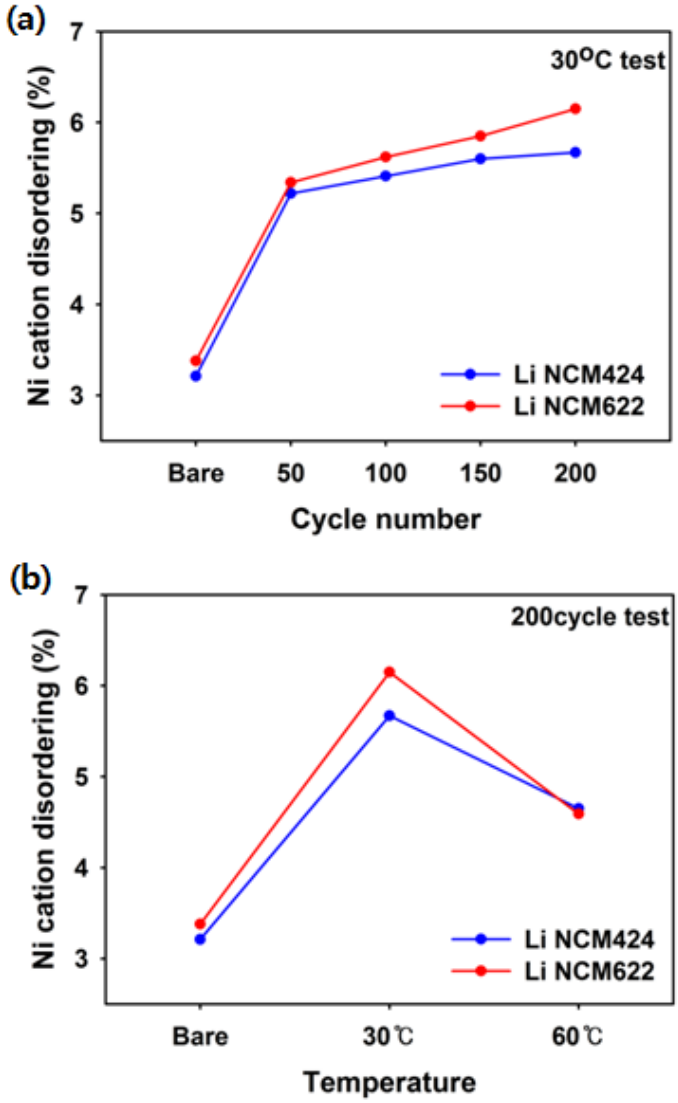

Figure 16. Plots of Ni disordering during cycling per (a) cycle number (30℃) and (b) temperature (200cycle)

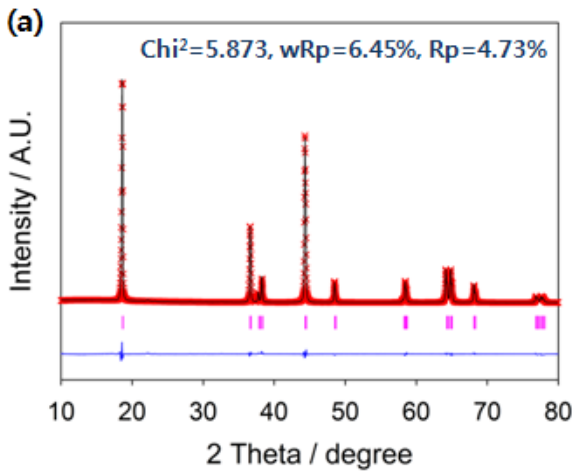

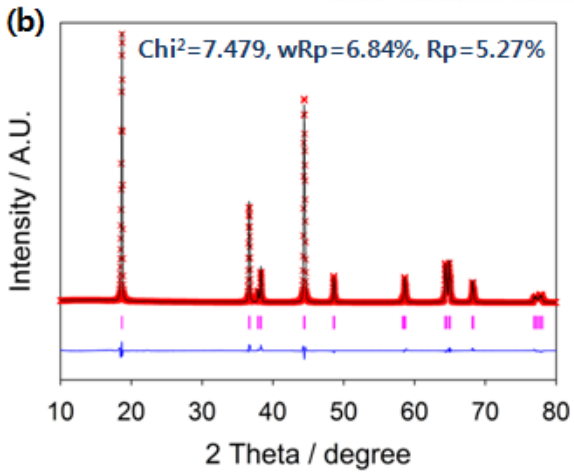

Sample	a / Å	c / Å	V / Å	c / a
424 Bare	2.873	14.271	102.000	4.968

α=β=90°, γ=120° , R-3m

Atom	Site	Occupancy	Uiso
Li1	3a	0.9679	0.01207
Ni2	3a	0.0321	0.01207
Li2	3b	0.0321	0.02254
Ni1	3b	0.3679	0.02254
Co	3b	0.2	0.02254
Mn	3b	0.4	0.02254
O	6c	1	0.03275

Sample	a / Å	c / Å	V / Å	c / a
622 Bare	2.871	14.224	101.545	4.954

α=β=90°, γ=120° , R-3m

Atom	Site	Occupancy	Uiso
Li1	3a	0.9662	0.01285
Ni2	3a	0.0338	0.01285
Li2	3b	0.0338	0.02236
Ni1	3b	0.5662	0.02236
Co	3b	0.2	0.02236
Mn	3b	0.2	0.02236
O	6c	1	0.03655

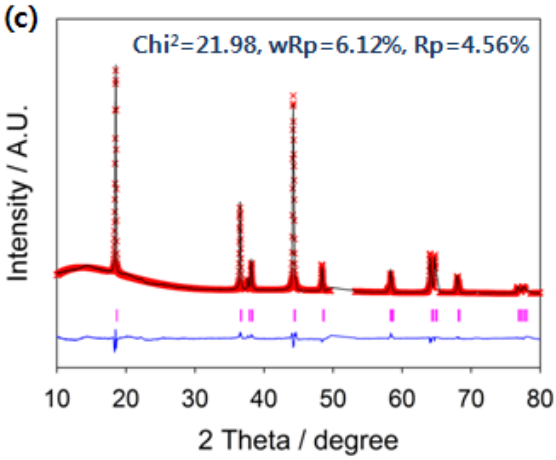

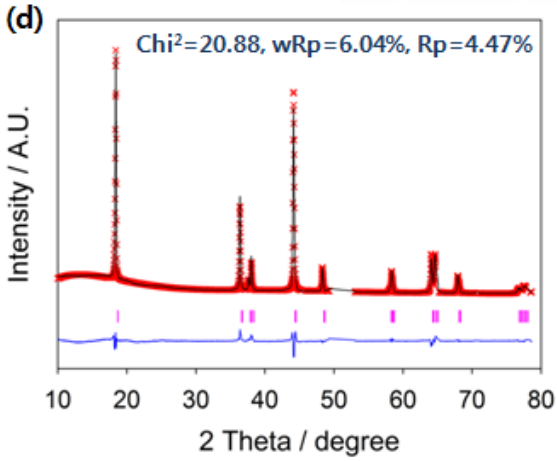

Sample	a / Å	c / Å	V / Å	c / a
424 Ed (30℃, 50cyc)	2.875	14.282	102.231	4.968

α=β=90°, γ=120° , R-3m

Atom	Site	Occupancy	Uiso
Li1	3a	0.9478	0.01213
Ni2	3a	0.0522	0.01213
Li2	3b	0.0522	0.02209
Ni1	3b	0.3478	0.02209
Co	3b	0.2	0.02209
Mn	3b	0.4	0.02209
O	6c	1	0.03212

Sample	a / Å	c / Å	V / Å	c / a
622 Ed (30℃, 50cyc)	2.872	14.229	101.669	4.954

α=β=90°, γ=120° , R-3m

Atom	Site	Occupancy	Uiso
Li1	3a	0.9466	0.01212
Ni2	3a	0.0534	0.01212
Li2	3b	0.0534	0.02271
Ni1	3b	0.5466	0.02271
Co	3b	0.2	0.02271
Mn	3b	0.2	0.02271
O	6c	1	0.03202

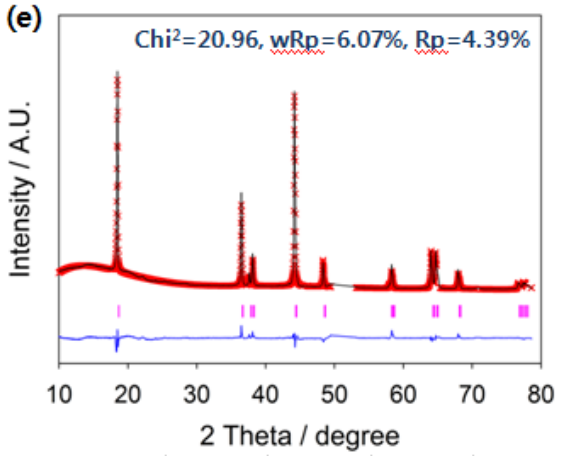

Sample	a / Å	c / Å	V / Å	c / a
424 Ed (30℃, 100cyc)	2.875	14.282	102.253	4.967

α=β=90°, γ=120° , R-3m

Atom	Site	Occupancy	Uiso
Li1	3a	0.9459	0.01210
Ni2	3a	0.0541	0.01210
Li2	3b	0.0541	0.02249
Ni1	3b	0.3459	0.02249
Co	3b	0.2	0.02249
Mn	3b	0.4	0.02249
O	6c	1	0.03252

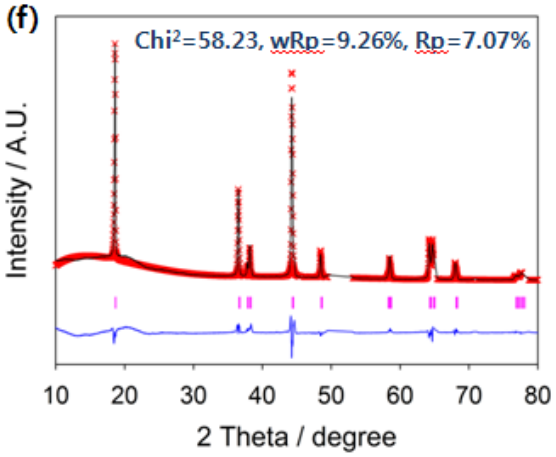

Sample	a / Å	c / Å	V / Å	c / a
622 Ed (30℃, 100cyc)	2.877	14.228	101.959	4.946

α=β=90°, γ=120° , R-3m

Atom	Site	Occupancy	Uiso
Li1	3a	0.9438	0.01269
Ni2	3a	0.0562	0.01269
Li2	3b	0.0562	0.02204
Ni1	3b	0.5438	0.02204
Co	3b	0.2	0.02204
Mn	3b	0.2	0.02204
O	6c	1	0.03211

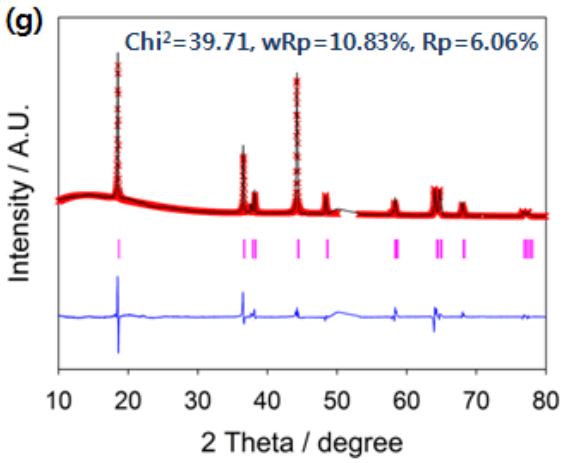

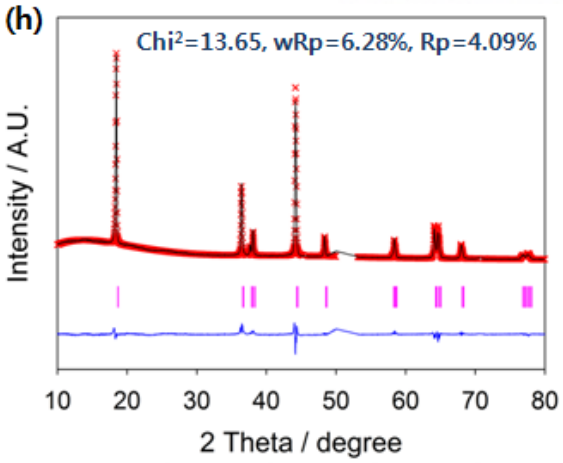

Sample	a / Å	c / Å	V / Å	c / a
424 Ed (30℃, 150cyc)	2.878	14.325	102.751	4.978

α=β=90°, γ=120° , R-3m

Atom	Site	Occupancy	Uiso
Li1	3a	0.9440	0.01270
Ni2	3a	0.0560	0.01270
Li2	3b	0.0560	0.02233
Ni1	3b	0.3440	0.02233
Co	3b	0.2	0.02233
Mn	3b	0.4	0.02233
O	6c	1	0.03291

Sample	a / Å	c / Å	V / Å	c / a
622 Ed (30℃, 150cyc)	2.873	14.234	101.713	4.955

α=β=90°, γ=120° , R-3m

Atom	Site	Occupancy	Uiso
Li1	3a	0.9415	0.01207
Ni2	3a	0.0585	0.01207
Li2	3b	0.0585	0.02290
Ni1	3b	0.5415	0.02290
Co	3b	0.2	0.02290
Mn	3b	0.2	0.02290
O	6c	1	0.03225

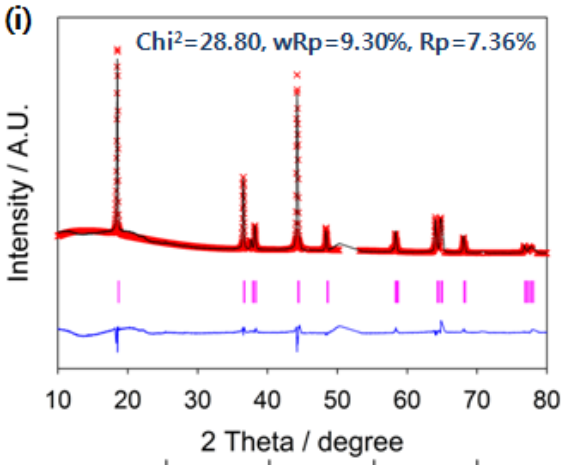

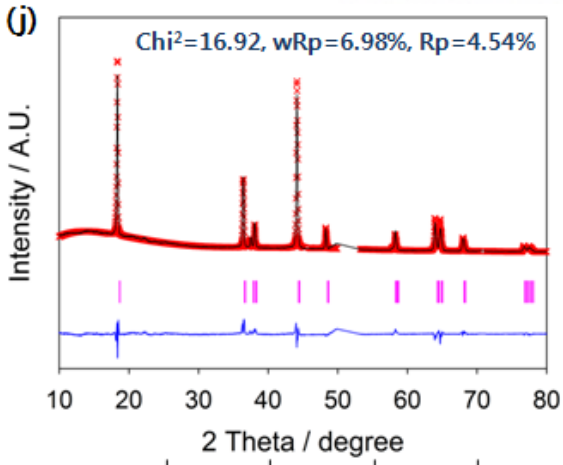

Sample	a / Å	c / Å	V / Å	c / a
424 Ed (30℃, 200cyc)	2.873	14.288	102.131	4.973

α=β=90°, γ=120° , R-3m

Atom	Site	Occupancy	Uiso
Li1	3a	0.9433	0.01258
Ni2	3a	0.0567	0.01258
Li2	3b	0.0567	0.02297
Ni1	3b	0.3433	0.02297
Co	3b	0.2	0.02297
Mn	3b	0.4	0.02297
O	6c	1	0.03213

Sample	a / Å	c / Å	V / Å	c / a
622 Ed (30℃, 200cyc)	2.870	14.279	101.864	4.975

α=β=90°, γ=120° , R-3m

Atom	Site	Occupancy	Uiso
Li1	3a	0.9385	0.01285
Ni2	3a	0.0615	0.01285
Li2	3b	0.0615	0.02274
Ni1	3b	0.5385	0.02274
Co	3b	0.2	0.02274
Mn	3b	0.2	0.02274
O	6c	1	0.03265

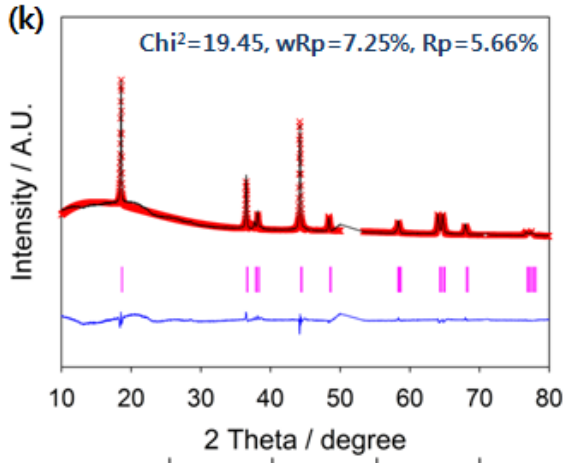

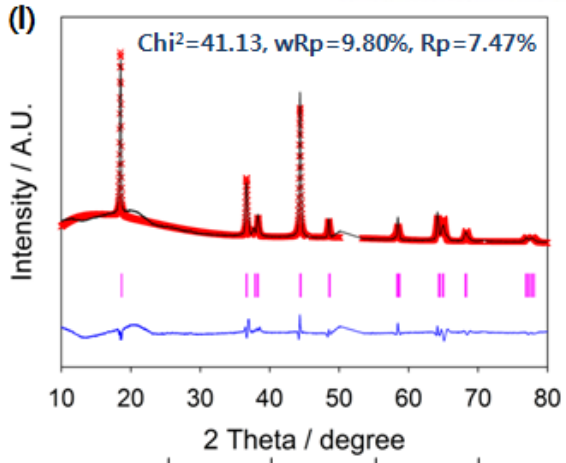

Sample	a / Å	c / Å	V / Å	c / a
424 Ed (60℃, 200cyc)	2.878	14.286	102.449	4.964

α=β=90°, γ=120° , R-3m

Atom	Site	Occupancy	Uiso
Li1	3a	0.9535	0.01213
Ni2	3a	0.0465	0.01213
Li2	3b	0.0465	0.02207
Ni1	3b	0.3535	0.02207
Co	3b	0.2	0.02207
Mn	3b	0.4	0.02207
O	6c	1	0.03273

Sample	a / Å	c / Å	V / Å	c / a
622 Ed (60℃, 200cyc)	2.864	14.282	101.466	4.986

α=β=90°, γ=120° , R-3m

Atom	Site	Occupancy	Uiso
Li1	3a	0.9541	0.01217
Ni2	3a	0.0459	0.01217
Li2	3b	0.0459	0.02210
Ni1	3b	0.5541	0.02210
Co	3b	0.2	0.02210
Mn	3b	0.2	0.02210
O	6c	1	0.03255

Figure 17. Rietveld refinement data patterns & lattice parameter value of (a) bare LiNCM 424 (424) (b) bare LiNCM 622 (622) (c) 50-cycled 424 at 30℃ (d) 50-cycled 622 at 30℃ (e) 100-cycled 424 at 30℃ (f) 100-cycled 622 at 30℃ (g) 150-cycled 424 at 30℃ (h) 150-cycled 622 at 30℃ (i) 200-cycled 424 at 30℃ (j) 200-cycled 622 at 30℃ (k) 200-cycled 424 at 60℃ (l)200-cycled 622 at 60℃

ULSAN NATIONAL INSTITUTE OF SCIENCE AND TECHNOLOGY

3-2. Chemical Mg-doping at Li layer

Synthesis characterization

To identify the structure during chemical Mg-doping process, Figure 18a shows the X-ray diffraction (XRD) patterns from bare Li NCM 424 to 300℃-heated $Mg_{0.025}Li_{0.95}$ NCM 424 powder. As you see in XRD patterns, each of powders maintains their R-3m layered structure. Although there are little bit shift and broaden peaks during several chemical reactions are progressed to layered Li NCM; Li elimination, Na insertion, and Na-Mg exchange, but in general, they have similar XRD patterns with no impurity peaks.

As other identification methods, Figure 18b-e shows the SEM image comparing between bare Li NCM 424 and 300℃-heated $Mg_{0.025}Li_{0.95}$ NCM 424 powder. As a result, they have almost same spherical morphology with similar particle size. Also, in magnified images (Figure 18c·e), both surfaces of spherical powders are similar, consisted of small-sized particles.

In ICP results, unlike the bare Li NCM 424 powder, there are small amount of Mg existed, although some Na ions are also detected (Figure 18f).

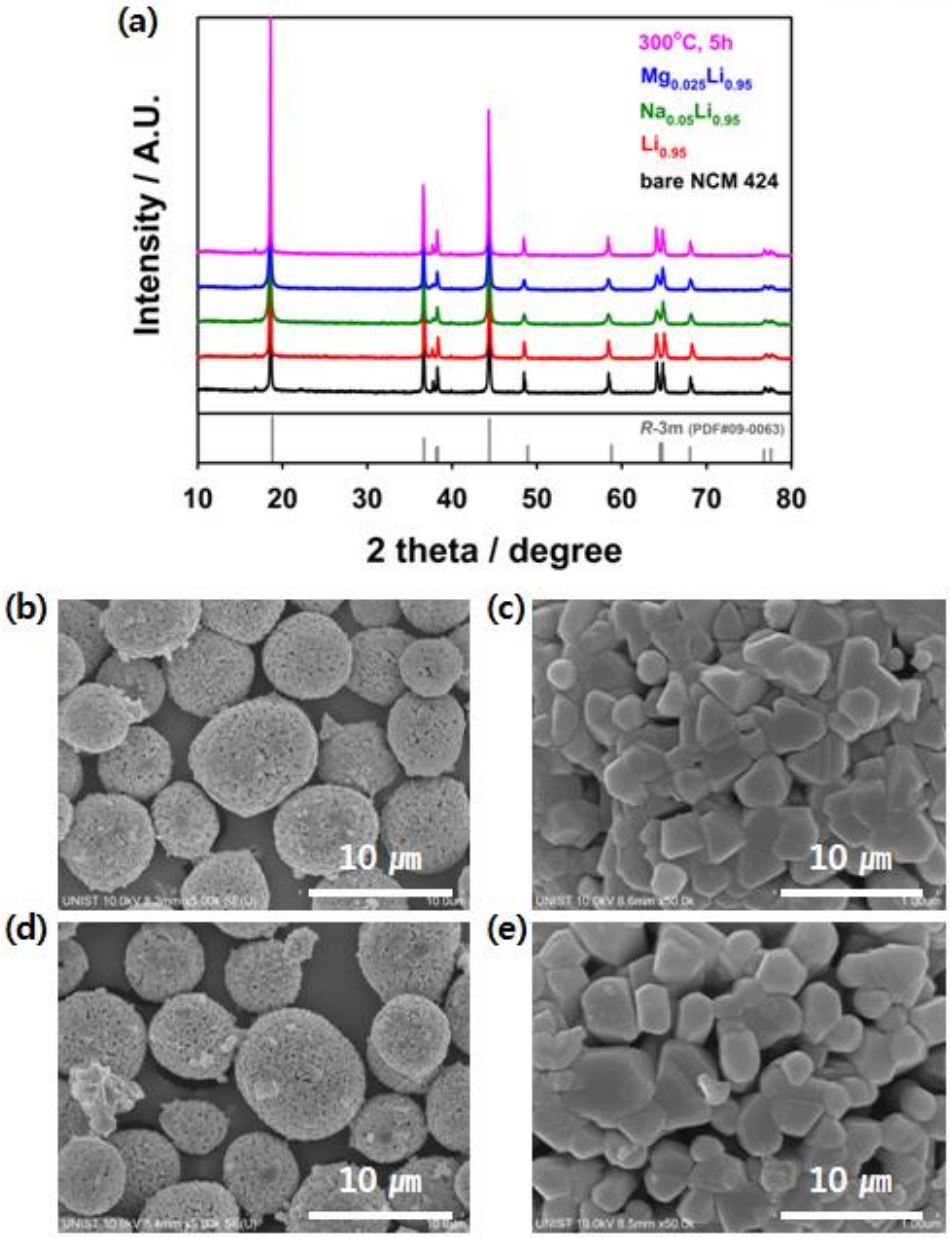

(f)

~NCM 424	Li	Na	Mg	NCM
Li (Bare)	1.070	X	X	1
$Mg_{0.025}Li_{0.95}$ (300°C, 5h)	0.947	0.035	0.026	1

Figure 18. (a) XRD patterns of chemical Mg-doping at Li layer process (b, c) SEM images of $LiNi_{0.4}Co_{0.2}Mn_{0.4}O_2$ and (d, e) $Mg_{0.025}Li_{0.95}Ni_{0.4}Co_{0.2}Mn_{0.4}O_2$ (f) ICP data of bare LiNCM 424 vs. Mg-doped LiNCM 424

However, only for using these measurements, we cannot determine that the Mg-ions are doped into the Li layer of layered Li NCM 424, definitely. And so, to clarify the Mg-doping at Li layer, additional data are needed; Rietveld refinement analysis of Mg-doped Li NCM powder (Figure 19).

In refinement analysis, as a result, our sample, $Mg_{0.025}Li_{0.95}$ NCM 424 powder has about 2.38% of Mg ions in Li layer, and its lattice parameter is increased about 0.02 Å along c axis after chemical Mg-doping process.

According to Rietveld refinement data, Mg ions can be existed in Li layer of layered Li NCM via chemical doping process, and small amount of Mg ions exist in Li layer of our sample. Combined these results, in conclusion, the small amount of Mg ions are doped into Li layer of our Li NCM 424.

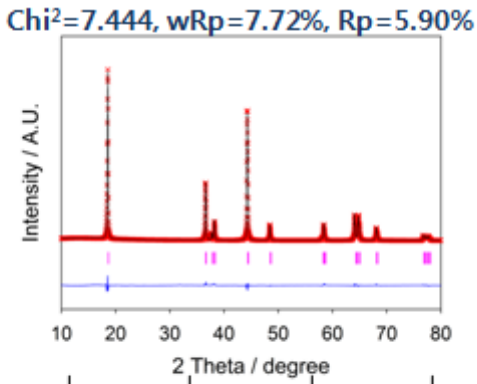

Sample	a / Å	c / Å	V / Å	c / a
424 Bare	2.873	14.271	102.000	4.968
$Mg_{0.025}$ 424	2.874	14.293	102.217	4.973

α=β=90°, γ=120° , R-3m

Atom	Site	Occupancy	Uiso
Li1	3a	0.9442	0.01222
Ni2	3a	0.0321	0.01222
Mg	3a	0.0238	0.01222
Li2	3b	0.0321	0.02276
Ni1	3b	0.3679	0.02276
Co	3b	0.2	0.02276
Mn	3b	0.4	0.02276
O	6c	1	0.03614

Figure 19. Rietveld refinement data patterns of $Mg_{0.025}Li_{0.95}Ni_{0.4}Co_{0.2}Mn_{0.4}O_2$ powder

Electrochemical performance

For electrochemical performance, Figure 20 shows a plot of discharge capacity as a function of cycle number for a bare and Mg-doped Li NCM 424 in Li half cell at 30℃. The initial discharge capacities of bare and Mg-doped samples are 128.7 and 130.0 mAh·g^{-1} at 1C rate, respectively. However, after 100 cycles, their discharge capacities are 105.3 and 124.5 mAh·g^{-1}, respectively. Also, bare and Mg-doped samples have 79.09 and 92.65% of capacity retention comparing the highest capacity during 100 cycles.

In supplementary, Figure 21 shows the V-profile and dQ/dV-V plot of bare and Mg-doped Li NCM cathode. In these plots, comparing with bare Li NCM 424, Mg-doped cathode has more stable V-profile with small polarization, and constant reaction potential after cycling.

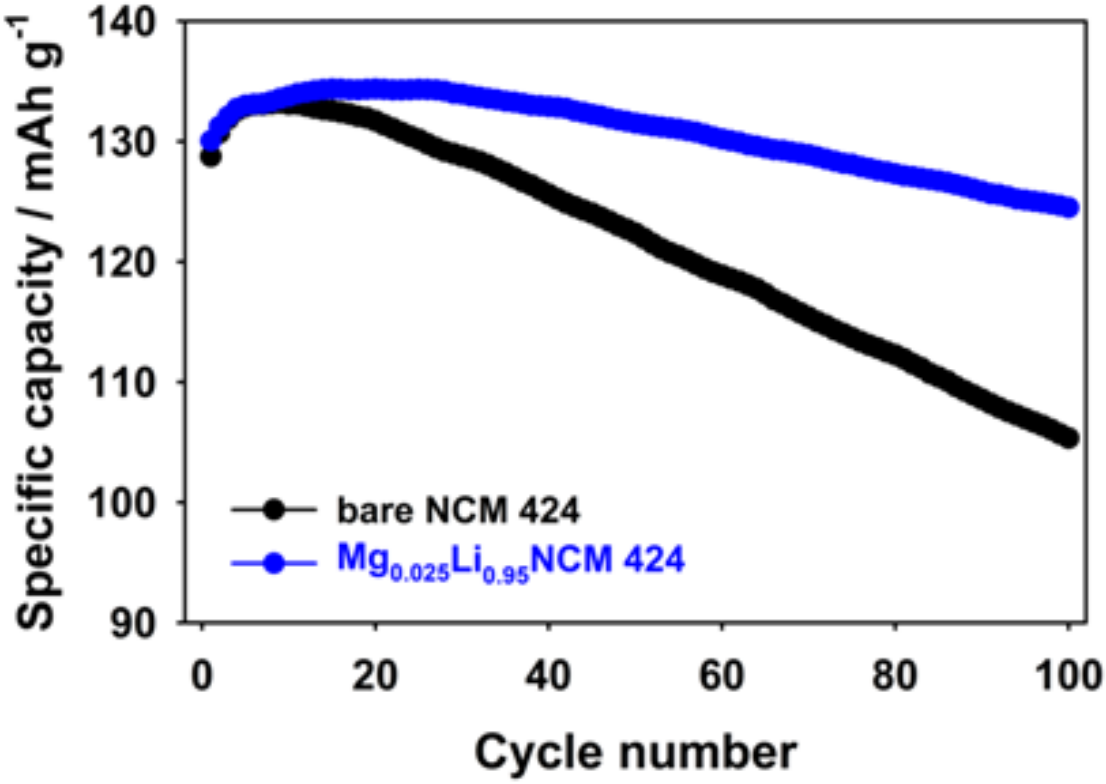

Figure 20. Cycleability of LiNCM 424 vs. Mg-doped LiNCM 424 half cell with Li metal anode at 30℃ (1C rate)

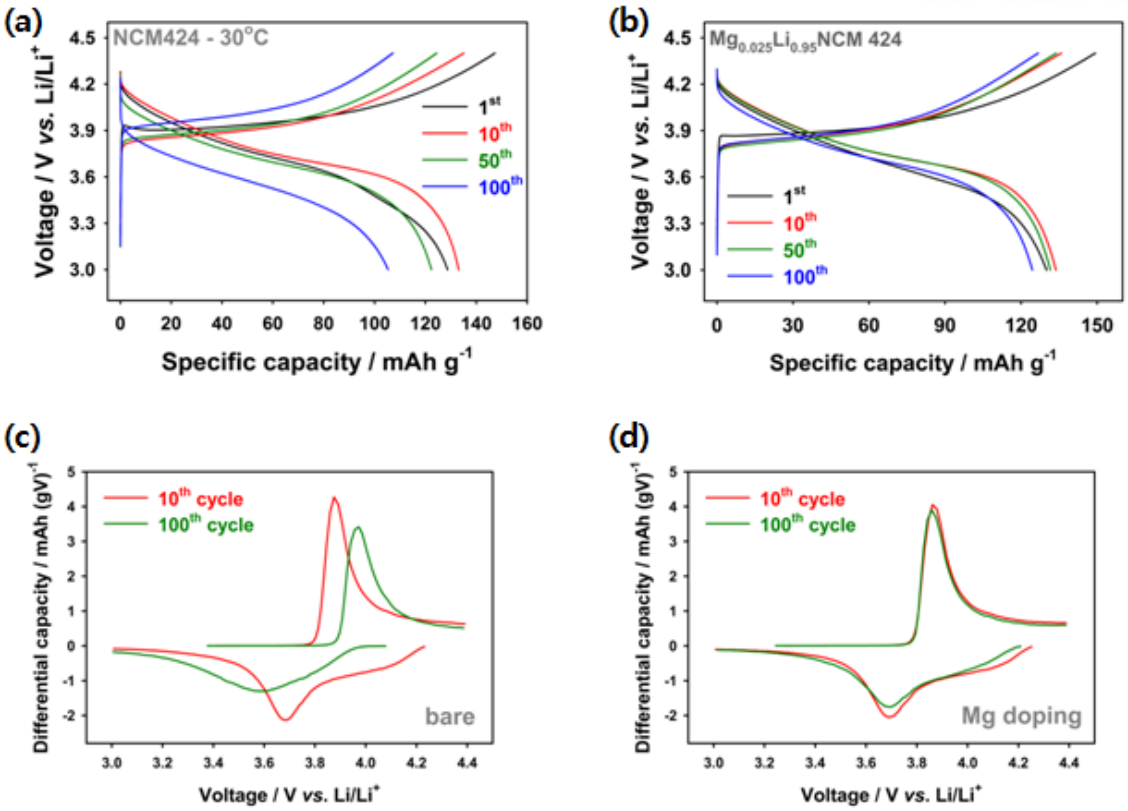

Figure 21. (a, b) Voltage profile of LiNCM 424 vs. Mg-doped LiNCM 424 half cell with Li metal anode at 30℃ (1C rate) (c, d) dQ/dV-V plot of 10th, 100th cycle at (a) and (b)

About this improvement, to observe the correlation with Ni disordering mechanism, Rietveld refinement method is used, and the results are shown in Figure 22. In result of Figure 22a, the degree of Ni disordering in 200-cycled Mg-doped Li NCM 424 has about 4.54%, as the median value of bare powder (3.21%) and 200-cycled Li NCM 424 cathode (5.67%). This means that Mg-doping at Li layer has somewhat inhibition of Ni disordering effect during cycling with structure stabilization.

(a)

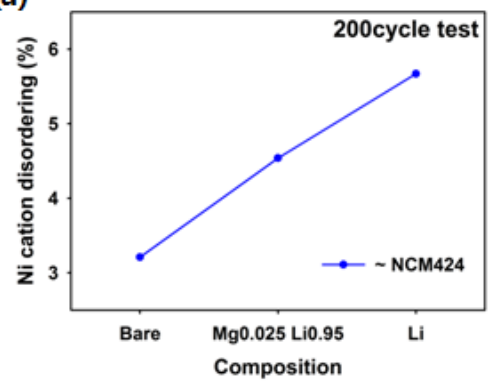

(b)

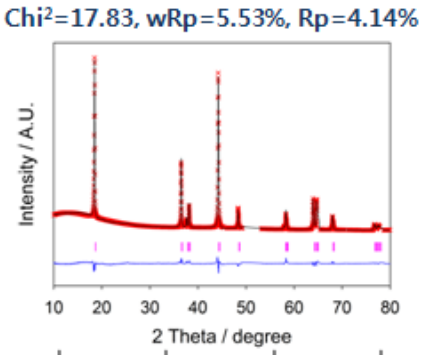

Sample	a / Å	c / Å	V / Å	c / a
424 Ed (30°C, 200cyc)	2.873	14.288	102.131	4.973
$Mg_{0.025}$ 424 (30oC, 200cyc)	2.874	14.293	102.264	4.973

α=β=90°, γ=120° , R-3m

Atom	Site	Occupancy	Uiso
Li1	3a	0.9442	0.01215
Ni2	3a	0.0454	0.01215
Mg	3a	0.0238	0.01215
Li2	3b	0.0454	0.02210
Ni1	3b	0.3679	0.02210
Co	3b	0.2	0.02210
Mn	3b	0.4	0.02210
O	6c	1	0.03284

Figure 22. (a) Plots of Ni disordering during cycling; bare vs. Mg-doping (b) Rietveld refinement data patterns of cycled $Mg_{0.025}Li_{0.95}Ni_{0.4}Co_{0.2}Mn_{0.4}O_2$ cathode

ULSAN NATIONAL INSTITUTE OF SCIENCE AND TECHNOLOGY

4. Conclusions

According to results, it is demonstrated that the Ni disordering, the bulk part problem, is one of the failure mechanisms related to capacity fading of layered Li NCM cathode.

Through XRD, SEM, ICP analysis, it is informed that our co-precipitated Li NCM 424·622 are well-synthesized, and half cell test shows various factors for severe capacity fading; Ni composition, temperature, and cycle number. About these factors, the degree of Ni disordering is measured using Rietveld refinement method. As results of refinement, except temperature, Ni disordering is affected by Ni composition & cycle number. Resultingly, higher the degree of Ni disordering with increased Ni composition & cycle number, more severe the capacity fading of Li NCM occurs, and this is the evidence for Ni disordering as one of failure mechanisms.

In addition, to improve Ni disordering & cycle performance, magnesium doping at Li layer is applied as the new type solution. Through TEM image and powder refinement, Mg doping at Li layer is successfully examined. Also, through the half cell test and refinement analysis, the effect of Mg doping is examined.

5. References

1. Megahed, S., Scrosati, B., 'Lithium-ion rechargeable batteries', *Journal of Power Sources*, **1994,** *51*, 79-104.

2. Yoshio, M., Brodd, R. J., Kozawa, A. (Eds.), 'Lithium-Ion Batteries: Science and Technologies', *Springer*, **2009.**

3. Nishi, Y,. 'Lithium ion secondary batteries; past 10 years and the future', *Journal of Power Sources*, **2001,** *100*, 101-106.

4. Tarascon, J. -M., Armand, M., 'Issues and challenges facing rechargeable lithium batteries', *Nature*, November **2001,** *414*, 15, 359-367.

5. Yang, X.Q., Sun, X., McBreen, J., 'New phases and phase transitions observed in $Li_{1-x}CoO_2$ during charge: in situ synchrotron X-ray diffraction sutdies', *Electrochemistry Communications*, **2000,** *2*, 100-103.

6. Shim, J. H., Lee, S., Park, S. S., 'Effects of MgO Coating on the Structural and Electrochemical Characteristics of $LiCoO_2$ as Cathode Materials for Lithium Ion Battery', *Chemistry of Materials*, **2014,** *26*, 2537-2543.

7. Okumura, T., Yamaguchi, Y., Shikano, M., Kobayashi, H., 'Correlation of lithium ion distribution and X-ray absorption near-edge structure in O3- and O2-lithium cobalt oxides from first-principle calculation', *Journal of Materials Chemistry*, **2012,** *22*, 17340-17348.

8. Reimers, Jan N., Dahn, J. R., 'Electrochemical and In Situ X-Ray Diffraction Studies of Lithium Intercalation in Li_xCoO_2', *Journal of The Electrochemical Society*, **1992**, *139* (8), 2091-2097.

9. Ohzuku, T., Ueda, A., 'Solid-State Redox Reactions of $LiCoO_2$ (R-3m) for 4 Volt Secondary Lihtium Cells', *Journal of The Electrochemical Society*, **1994,** *141* (11), 2972-2977.

10. Amatucci, G. G., Tarascon, J. M., Klein, L. C., 'CoO_2, The End Member of the Li_xCoO_2 Solid Solution', *Journal of The Electrochemical Society*, **1996,** *143* (3), 1114-1123.

11. Cho, J., Kim, Y. J., Park, B., '$LiCoO_2$ Cathode Material That Does Not Show a Phase Transition from Hexagonal to Monoclinic Phase', *Journal of The Electrochemical Society*, **2001,** *148* (10), A1110~A1115.

12. Lu, Z. H., Macneil, D. D., Dahn, J. R., 'Layered $Li[Ni_xCo_{1-2x}Mn_x]O_2$ cathode Materials for Lithium-Ion Batteries', *Electrochemical and Solid-State Letters*, **2001,** *4*, A200-A203.

13. Shaju, K. M., Subba Rao, G. V., Chowdari, B. V. R., 'Performance of layered $Li(Ni_{1/3}Co_{1/3}Mn_{1/3})O_2$ as cathode for Li-ion batteries', *Electrochimica Acta*, **2002,** *48*, 145-151.

14. Belharouak, I., Sun, Y. -K., Liu, J., Amine, K., '$Li(Ni_{1/3}Co_{1/3}Mn_{1/3})O_2$ as a suitable cathode for high power application', *Journal of Power Sources*, **2003,** *123*, 247-252.

15. Kim, J. -M., Chung, H. -T., 'The first cycle characteristics of $Li[Ni_{1/3}Co_{1/3}Mn_{1/3}]O_2$ charged up to 4.7V', *Electrochemica Acta*, **2004,** *49*, 937-944.

ULSAN NATIONAL INSTITUTE OF SCIENCE AND TECHNOLOGY

16. Shin, Y. -J., Choi, W. -J., Hong, Y. -S., Yoon, S., Ryu, K. S., Chang, S. H., 'Investigation on the microscopic features of layered oxide $Li[Ni_{1/3}Co_{1/3}Mn_{1/3}]O_2$ and their influences on the cathode properties', *Solid State Ionics*, **2006,** *177*, 515-521.

17. Liang, Y., Han, X., Zhou, X., Sun, J., Zhou, Y., 'Significant improved electrochemical performance of $Li(Ni_{1/3}Co_{1/3}Mn_{1/3})O_2$ cathode on volumetric energy density and cycling stability at high rate', *Electrochemistry Communications*, **2007,** *9*, 965-970.

18. He, P., Wang, H., Qi, L., Osaka, T., 'Electrochemical characteristics of layered $LiNi_{1/3}Co_{1/3}Mn_{1/3}O_2$ and with different synthesis conditions', *Journal of Power Sources*, **2006,** *160*, 627-632.

19. Luo, X., Wang, X., Liao, L., Gamboa, S., Sebastian, P. J., 'Synthesis and characterization of high tap-density layered $Li[Ni_{1/3}Co_{1/3}Mn_{1/3}]O_2$ cathode material via hydroxide co-precipitation', *Journal of Power Sources*, **2006,** *158*, 654-658.

20. Li, D. -C., Muta, T., Zhang, L. -Q., Yoshio, M., Noguchi, H., 'Effect of synthesis method on the electrochemical performance of $LiNi_{1/3}Mn_{1/3}Co_{1/3}O_2$', *Journal of Power Sources*, **2004,** *132*, 150-155.

21. Zhang, S., Deng, C., Yang, S. Y., Niu, H., 'An improved carbonate co-precipitation method for the preparation of spherical $Li[Ni_{1/3}Co_{1/3}Mn_{1/3}]O_2$ cathode material', *Journal of Alloys and Compounds*, **2009,** *484*, 519-523.

22. Reddy, M. V., Subba Rao, G. V., Chowdari, B. V. R., 'Synthesis by molten salt and cathodic properties of $Li(Ni_{1/3}Co_{1/3}Mn_{1/3})O_2$', *Journal of Power Sources*, **2006,** *159*, 263-267.

23. Park, S. -H., Shin, H. -S., Myung, S. -T., Yoon, C. S., Amine, K., Sun, Y. -K., 'Synthesis of Nanostructured $Li[Ni_{1/3}Co_{1/3}Mn_{1/3}]O_2$ via a Modified Carbonate Process', *Chemistry of Materials*, **2005,** *17*, 6-8.

24. Zhang, S., Qiu, X., He, Z., Weng, D., Zhu, W., 'Nanoparticled $Li(Ni_{1/3}Co_{1/3}Mn_{1/3})O_2$ as cathode material for high-rate lithium-ion batteries', *Journal of Power Sources*, **2006,** *153*, 350-353.

25. Liu, J., Qiu, W., Yu, L., Zhao, H., Li, T., 'Synthesis and electrochemical characterization of layered $Li(Ni_{1/3}Co_{1/3}Mn_{1/3})O_2$ cathode materials by low-temperature solid-state reaction', *Journal of Alloys and Compounds*, **2008,** *449*, 326-330.

26. Deng, C., Zhang, S., Ma, L., Sun, Y. H., Yang, S. Y., Fu, B. L., Liu, F. L., Wu, Q., 'Effects of precipitator on the morphological, structural and electrochemical characteristics of $Li[Ni_{1/3}Co_{1/3}Mn_{1/3}]O_2$ prepared via carbonate coprecipitation', *Journal of Alloys and Compounds*, **2011,** *509*, 1322-1327.

27. Delmas, C., Saadoune, I., Rougier, A., 'The cycling properties of the $Li_xNi_{1-y}Co_yO_2$ electrode', *Journal of Power Sources*, **1993,** *44*, 595-602.

28. Arai, H., Okada, S., Sakurai, Y., Yamaki, J., 'Electrochemical and thermal behavior of $LiNi_{1-z}M_zO_2$ (M = Co, Mn, Ti)', *Journal of The Electrochemical Society*, **1997,** *144*, 3117-3125.

29. Shim, J., Kostecki, R., Richardson, T., Song, X., Striebel, K. A., 'Electrochemical analysis for cycle performance and capacity fading of a lithium-ion battery cycled at elevated temperature', *Journal of Power Sources*, **2002,** *112*, 222-230.

ULSAN NATIONAL INSTITUTE OF SCIENCE AND TECHNOLOGY

30. Bang, H. J., Joachin, H., Yang, H., Amine, K., Prakash, J., 'Contribution of the structural changes of $LiNi_{0.8}Co_{0.15}Al_{0.05}O_2$ cathodes on the exothermic reactions in Li-ion cells', *Journal of The Electrochemical Society*, **2006,** *153*, A731-A737.

31. Zhong, Q. M., von Sacken, U., 'Crystal structures and electrochemical properties of $LiAl_yNi_{1-y}O_2$ solid solution', *Journal of Power Sources*, **1995,** *54*, 221-223.

32. Gao, Y. A., Yakovleva, M. V., Ebner, W. B., 'Novel $LiNi_{1-x}Ti_{x/2}Mg_{x/2}O_2$ compounds as cathode materials for safer lithium-ion batteries', *Electrochemical and Solid-State Letters*, **1998,** *1*, 117-119.

33. Delmas, C., Menetrier, M., Croguennec, L., Saadoune, I., Rougier, A., Pouillerie, C., Prado, G., Grune, M., Fournes, L., 'An overview of the $Li(Ni,M)O_2$ systems: synthesis, structures and properties', *Electrochimica Acta*, **1999,** *45*, 243-253.

34. Chebiam, R. V., Prado, F., Manthiram, A., 'Structural instability of delithiated $Li_{1-x}Ni_{1-y}Co_yO_2$ cathodes', *Journal of The Electrochemical Society*, **2001,** *148*, A49-A53.

35. Komaba, S., Kumagai, N., Kataoka, Y., 'Influence of manganese(Ⅱ), cobalt(Ⅱ), and nickel(Ⅱ) additives in electrolyte on performance of graphite anode for lithium-ion batteries', *Electrochimica Acta*, **2002,** *47*, 1229-1239.

36. Noh, H. -J., Youn, S., Yoon, C. S., Sun, Y. -K., 'Comparison of the structural and electrochemical properties of layered $Li[Ni_xCo_yMn_z]O_2$ (x = 1/3, 0.5, 0.6, 0.7, 0.8 and 0.85) cathode material for lithium-ion batteries', *Journal of Power Sources*, **2013,** *233*, 121-130.

37. Jung, S. -K., Gwon, H., Hong, J., Park, K. -Y., Seo, D. -H., Kim, H., Hyun, J., Yang, W., Kang, K., 'Understanding the Degradation Mechanisms of $LiNi_{0.5}Co_{0.2}Mn_{0.3}O_2$ Cathode Material in Lithium Ion Batteries', *Advanced Energy Materials*, **2014,** *4*, 1300787.

38. Woo, S. H., Lim, H. -W., Jeon, S., Travis, J. J., George, S. M., Lee, S. -H., Jo, Y. N., Song, J. H., Jung, Y. S., Hong, S. Y., Choi, N. -S., Lee, K. T., 'Ion-Exchangeable Functional Binders and Separator for High Temperature Performance of $Li_{1.1}Mn_{1.86}Mg_{0.04}O_4$ Spinel Electrodes in Lithium Ion Batteries', *Journal of The Electrochemical Society*, **2013,** *160* (11), A2234-A2243.

39. Matsumoto, K., Kuzuo, R., Takeya, K., Yamanaka, A., 'Effects of CO_2 in air on Li deintercalation from $LiNi_{1-x-y}Co_xAl_yO_2$', *Journal of Power Sources*, **1999,** *81-82*, 558-561.

40. Noh, M., Lee, Y., Cho, J., 'Water Adsorption and Storage Characteristics of Optimized $LiCoO_2$ and $LiNi_{1/3}Co_{1/3}Mn_{1/3}O_2$ Composite Cathode Material for Li-Ion Cells', *Journal of The Electrochemical Society*, **2006,** *153* (5), A935-A940.

41. Eom, J., Kim, M. G., Cho, J., 'Storage Characteristics of $LiNi_{0.8}Co_{0.1+x}Mn_{0.1-x}O_2$ (x = 0, 0.03, and 0.06) Cathode Materials for Lithium Batteries', *Journal of The Electrochemical Society*, **2008,** *155* (3), A239-A245.

42. Choi, S., Manthiram, A., 'Factors Influencing the Layered to Spinel-like Phase Transition in Layered Oxide Cathodes', *Journal of The Electrochemical Society*, **2002,** *149* (9) A1157-A1163.

43. Bak, S. -M., Hu, E., Zhou, Y., Yu, X., Senanayake, S. D., Cho, S. -J., Kim, K. -B., Chung, K. Y., Yang, X. -Q., Nam, K. -W., 'Structural Changes and Thermal Stability of Charged $LiNi_xMn_yCo_zO_2$ Cathodes Materials Studied by Combined In Situ Time-Resolved XRD and

ULSAN NATIONAL INSTITUTE OF SCIENCE AND TECHNOLOGY

Mass Spectroscopy', *ACS applied Materials & Interfaces*, **2014,** xxx-xxx.

44. Breger, J., Meng, Y. S., Hinuma, Y., Kumar, S., Kang, K., Shao-Horn, Y., Ceder, G., Grey, C. P., 'Effect of High Voltage on the Structure and Electrochemistry of $LiNi_{0.5}Mn_{0.5}O_2$: A Joint Experimental and Theoretical Study', *Chemistry of Materials*, **2006,** *18*, 4768-4781.

45. Xu, H., Deng, S., Chen, G., 'Improved electrochemical performance of $Li_{1.2}Mn_{0.54}Ni_{0.13}Co_{0.13}O_2$ by Mg doping for lithium ion battery cathode material', *Journal of Materials Chemistry A*, **2014,** *2*, 15015-15021.

46. Lee, M. -H., Kang, Y. -J., Myung, S. -T., Sun, Y. -K., 'Synthetic optimization of $Li[Ni_{1/3}Co_{1/3}Mn_{1/3}]O_2$ via co-precipitation', *Electrochimica Acta*, **2004,** *50*, 939-948.

47. Sun, Y. -K., Lee, B. -R., Noh, H. -J., Wu, H., Myung, S. -T., Amine, K., 'A novel concentration-gradient $Li[Ni_{0.83}Co_{0.07}Mn_{0.10}]O_2$ cathode material for high-energy lithium-ion batteries', *Journal of Materials Chemistry*, **2011,** *21*, 10108-10112.

48. Kim, W. -S., Kim, S. -B., Jang, J. C., Lim, H. H., See, Y. S., 'Remarkable improvement in cell safety for $Li[Ni_{0.5}Co_{0.2}Mn_{0.3}]O_2$ coated with $LiFePO_4$', *Journal of Alloys and Compounds*, **2010,** *492*, L87-L90.

49. Kim, S. -B., Lee, K. J., Choi, W. J., Kim, W. -S., Jang, I. C., Lim, H. H., Lee, Y. S., 'Preparation and cycle performance at high temperature for $Li[Ni_{0.5}Co_{0.2}Mn_{0.3}]O_2$ coated with $LiFePO_4$', *Journal of Solid State Electrochemistry*, **2010,** *14*, 919-922.

50. Wang, D., Huang, Y., Huo, Z., Chen, L., 'Synthesize and electrochemical characterization of Mg-doped Li-rich layered $Li[Li_{0.2}Ni_{0.2}Mn_{0.6}]O_2$ cathode material', *Electrochemica Acta*, **2013,** *107*, 461-466.